ABSTRACT

LIM, SANIEL DONG. Ocean Compressed Air Energy Storage (OCAES) Integrated with Offshore Renewable Energy Sources. (Under the direction of Dr. Andre P. Mazzoleni.)

Because of the worldwide efforts to reduce the dependency on fossil fuels, demand for renewable energy generation has been raised significantly in recent years. Since the intermittency of these renewable energy sources requires significant energy storage capacity, compressed air energy storage (CAES) technology is studied in this thesis as a feasible option for utility-scale energy storage systems.

The main goal of the research is to develop a new concept for a zero-emission ocean-based CAES system. In addition to an introduction to existing and advanced CAES systems, a thermodynamic analysis of the existing CAES systems is presented. After that, a schematic of an ocean compressed air energy storage (OCAES) system is proposed along with a discussion of its advantages and geographical aspects (note: OCAES is sometimes referred to as “Offshore Compressed Air Energy Storage”). In addition to OCAES systems which make use of auxiliary power from natural gas, a zero-emission OCAES system is proposed, which makes use of thermal energy storage (TES). TES has been widely used in conjunction with solar energy generation since the 1980s. Based on a thermodynamic analysis of the existing CAES system, a thermodynamic model of an adiabatic OCAES system is demonstrated and used to estimate the required specifications of various OCAES subsystems. The results show that an adiabatic OCAES making use of TES which does not require the burning of fossil fuels is feasible thermodynamically.

An OCAES system presents a promising alternative to land-based CAES systems, but several new challenges need to be addressed before OCAES systems can be successfully implemented, such as buoyancy, anchoring, and loads due to ocean currents. To address some of these issues, finite element analyses of an underwater air container are conducted where the container is exposed to extreme loading conditions, such as might be experience during a hurricane. The results of these analyses can be used to aid in the design of the system, including anchoring and/or mooring.

To summarize, this thesis presents the conceptual design of an OCAES system as well as thermodynamic analyses of both CAES and OCAES systems. In addition, the structural behavior of an underwater air storage container exposed to ocean currents are evaluated through computational finite element simulations.

Ocean Compressed Air Energy Storage (OCAES) Integrated with Offshore Renewable Energy Sources

by
Saniel Dong Lim

A thesis submitted to the Graduate Faculty of
North Carolina State University
in partial fulfillment of the
requirements for the degree of
Master of Science

Mechanical Engineering

Raleigh, North Carolina

2013

APPROVED BY:

_____
Dr. Andre P. Mazzoleni
Committee Chair

_____ _____
Dr. Paul I. Ro Dr. Joseph F. DeCarolis

BIOGRAPHY

Saniel Lim was born in Ann Arbor, MI on April 7, 1983. He graduated with a Bachelor of Science in Mechanical engineering from Ajou University in Suwon, Korea. After coming back to the United States, he began his Master of Science program in Mechanical engineering at North Carolina State University in 2011. In August 2011, he started research on compressed air energy storage under the direction of Dr. Andre Mazzoleni.

ACKNOWLEDGMENTS

Firstly, I would thank my advisor, Dr. Andre Mazzoleni, for giving me an opportunity to work on this topic and for his supervision and encouragement during my master's program. I was lucky to have an advisor who always led me on the right path of research with his critical advice and his kind guidance.

I would personally like to thank Dr. Paul Ro for his assistance during my graduate years. Your counsel before I was admitted to the graduate school was invaluable and it has been a pleasure that I happened to work on this project with you.

I would also thank Dr. Joseph DeCarolis for serving on my committee. It is a great honor for me to present my research to someone who has worked on this project and on related topics for many years.

I am very grateful to my friends in the States and Korea. Their constant encouragement and support always keep me positive and hopeful.

Last but not the least, my deepest gratitude goes to my family. Without your endless love and continuous support, I could not have even started my graduate studies.

TABLE OF CONTENTS

LIST OF TABLES

LIST OF FIGURES

CHAPTER 1

INTRODUCTION

1.1. Background and Motivation

When the Industrial Revolution took place between the 18th and 19th centuries, fossil fuels became the primary energy source and their consumption has risen dramatically. According to the Annual Energy Review 2011 by the U.S. Energy Information Administration, the fossil fuel share of total energy consumption in the U.S. is 82 % (EIA, 2011). Although fossil fuels are readily available at present, there is not an unlimited supply of fossil fuels, so eventually they will be depleted. Moreover, since there are environmental issues associated with burning fossil fuels, efforts to reduce the dependency on fossil fuels are increasingly gaining momentum worldwide. Demand for renewable energy generation has been raised significantly in recent years, these renewable energy sources, however, have a critical disadvantage, namely unpredictability of supply. For example, weather and climate can often affect renewable energy sources such as wind, solar, tidal, and wave, or these renewables would likely be strong at off peak times. Considering nuclear power generation a base load supply, the energy from renewables must be dispatchable to compete and replace conventional fossil fuels (grid operators can then make use of it for load leveling and emergency backup).

In order to provide high quality power from renewable energy sources to the grid, a bulk energy storage system will be required as a buffer. Numerous energy storage methods are being developed with various performances in terms of power ratings and discharge times. Figure 1.1 shows the comparison of the power rating and the discharge time for various energy storage systems. Battery storage, flywheel energy storage (FES) and pumped hydro energy storage (PHS) are the most common types of energy storage systems currently in use or in development. Battery storage systems and FES are efficient and quick-responding, but they are expensive and small-scale so that they usually serve as an emergency power backup system and a power quality system. PHS is large-scale, but the construction is costly and subject to geographic limitations (Arsie, Marano, Rizzo, & Moran, 2009).

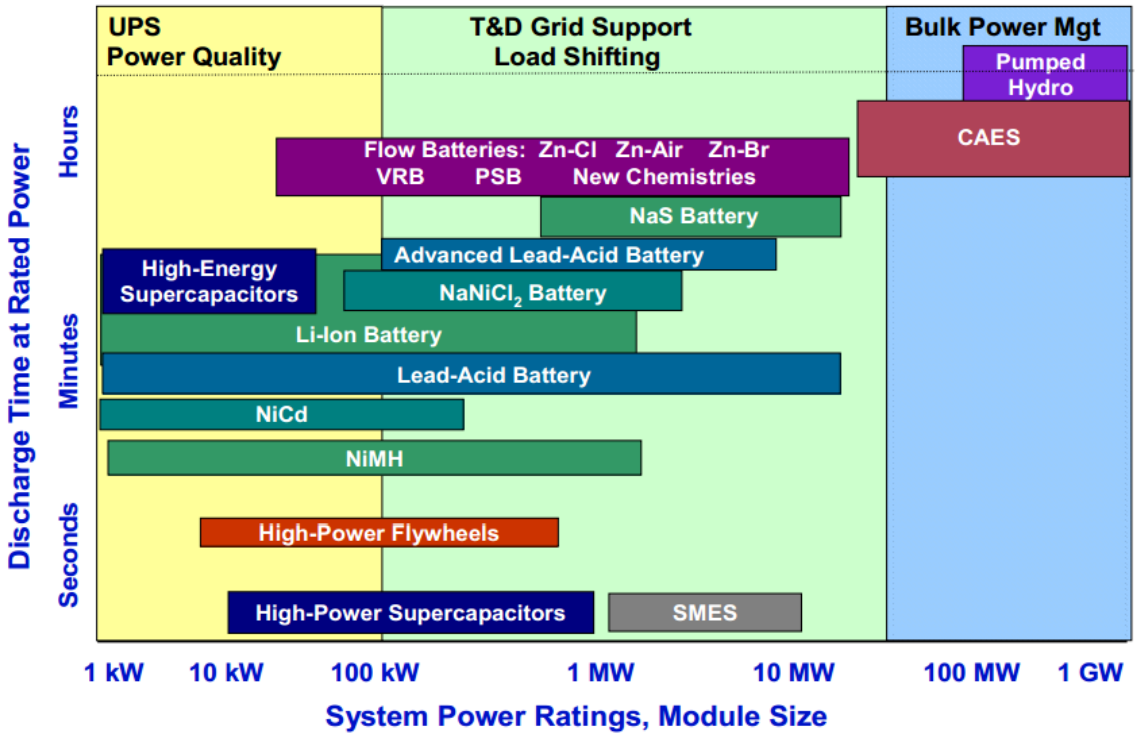

Figure 1.1 Comparison of power ratings and discharge time of various energy storage systems (Rastler, 2010)

As a near-term utility-scale energy storage technology, compressed air energy storage (CAES) is worth studying because CAES is a scalable, economical, and proven technology. In North Carolina, efforts to utilize the potential of offshore energy have begun and ocean compressed air energy storage (OCAES) systems are being examined as an energy storage option (note: OCAES is sometimes referred to as “Offshore Compressed Air Energy Storage”). Installation of an air storage container on the seabed not only avoids the environmental and safety issues of an inland facility, but also takes advantage of the hydrostatic pressure at the ocean floor which can keep the compressed air under storage at high pressure without the need for an expensive pressure vessel or underground cavern.

1.2. Scope of Work

The primary goal of this research is to propose a feasible OCAES system design for the coast of North Carolina where offshore renewable energy generations have been considered. In order to present the comprehensive system layout, the research topic is mainly divided into three parts: existing CAES systems, OCAES system with TES, and underwater air storage container. The following objectives of this thesis are achieved in each chapter: (1) to introduce the CAES as an attractive energy storage technology to enhance the capacity factors of renewable energy generations, (2) to analyze the thermodynamic performance of existing CAES plants, (3) to develop an overall conceptual design of OCAES in addition to discussing geographical and systematic advantages of OCAES, (4) to investigate the thermodynamic performance of the proposed OCAES system, and (5) to conduct finite element analysis of structural behaviors of an air storage structure in seabed flow field.

CHAPTER 2

COMPRESSED AIR ENERGY STORAGE SYSTEM

2.1. Introduction

Compressed air energy storage (CAES) is the one of the utility-scale energy storage technologies that is proven to be used in the industry. The other is pumped hydro energy storage. CAES system stores low-cost off-peak electric energy in an underground cavern in the form of compressed air and dispatches electric energy during peak hours. There are two commercial CAES systems which have been built and operated in Germany and the United States. In 1978, the first CAES plant began operation in Huntorf, Germany. The second CAES was built in McIntosh, Alabama in 1991.

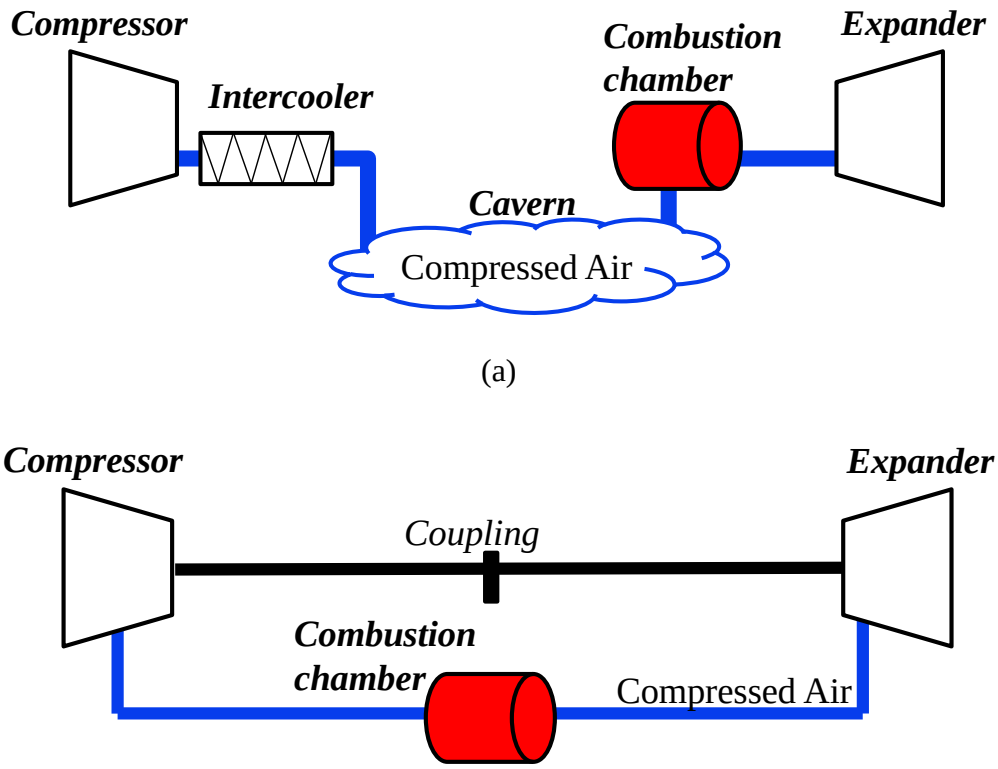

Figure 2.1 Schematics of (a) CAES and (b) gas turbine

As seen in Figure 2.1, a compressor, turbine, and combustion chamber are the principal sub-components in a CAES system. Although the arrangement of a CAES system is analogous to that of a gas turbine generation system, the actual operating procedures can be distinguished. In a gas turbine operating in steady state mode, ambient air is compressed adiabatically and heated subsequently by fuel energy within a combustion chamber. The heated and pressurized air is then exhausted from the turbine, rotating an expander which drives a generator or other load device. A compressor and turbine are connected by a shaft by which a

third to a half of generated power by the turbine is used to operate the compressor. In a CAES system, both a compressor and expander trains are connected to a motor-generator unit by means of a clutch. Therefore, the compression and expansion cycles runs separately. The CAES system works by using electricity to compress ambient air, which is then cooled down before it is stored in an underground cavern instead of being heated in the combustion chamber. During on-peak times, electricity is regenerated by recovering compressed air from the storage chamber, combining it with natural gas in a combustion chamber, and exhausting the combustion products through a turbine.

The conventional CAES systems have been operated as a spinning reserve, which is defined as unloaded generation ready to serve additional demand (Rebours & Kirschen, 2005). The existing CAES systems are able to ramp up to full capacity within 10 minutes and the availability and reliability for both existing CAES plants are reported to be over 90% and 99%, respectively (Steta, 2010).

For the storage in which the compressed air is collected, the two conventional CAES plants make use of solution-mined salt caverns. There are many different reservoir options that have been studied for the most suitable storage option geologically and economically; steel pipes, depleted gas or oil reservoirs, mines, rock caverns, and aquifers (Boehme, Cammaert, McCurry, Judt, & Deckers, 2007; Favret, 2004). Yet these reservoir options have not been built for a CAES system.

In this chapter, the utility-scale energy storage option which is making use of compressed air is introduced. In addition to the necessity of CAES, advanced turbomachinery technologies for CAES systems are discussed. The thermodynamic performance of the existing McIntosh

CAES facility is also evaluated, which will be used for designing an ocean-based CAES system in the next chapter.

2.2. Existing CAES Systems

The two conventional CAES systems, in Huntorf, Germany and in McIntosh, AL, are currently in operation. These two facilities have been successfully served main functions of energy storage for over 35 years and 22 years, yielding actual long-term operational data. Figure 2.2 shows the aerial views of the Huntorf plant and the McIntosh plant. Table 2.1 presents the specifications of the existing CAES systems (Basler & Zaugg, 1985; Crotogino, Mohmeyer, & Scharf, 2001; Desai, Gonzalez, Pemberton, & Rathjen, 2005; E.ON, 2013; A. J. Pimm, 2011; Pollak, 1994a; Schainker, Pollak, & Mehta, 1993; Singal, 1984; Steta, 2010; Tuschy, 2002).

(a)

(b)

Figure 2.2 Aerial views of (a) the Huntorf CAES plant and (b) the McIntosh CAES plant (Abele, 2011)

Table 2.1: Comparison of the existing CAES plants

Parameter	Huntorf (Germany)	McIntosh AL (USA)
Build Year	1978 (rebuilt in 2007)	1991
Power Capacity Turbine Compressor	 321 MW (2 hours) 62 MW (12 hours)	 110 MW (26 hours) 53 MW (41 hours)
Cavern Volume	310,000 m^3	560,000 m^3
Mass Flow Rate Turbine Compressor	 455 kg/s 108 kg/s	 157 kg/s 94 kg/s
Cavern Air Pressures Discharged (Min) Charged (Max)	 4.2 MPa 7.2 MPa	 4.6 MPa 7.4 MPa
High Pressure Turbine Air Pressure Air Temperature	 4.13 MPa 490 ℃	 4.4 MPa 540 ℃
Low Pressure Turbine Air Pressure Air Temperature	 1.28 MPa 945 ℃	 1.6 MPa 870 ℃
Fuel	Gas	Gas/Oil
Recuperator	No	Yes
Heat Rate	5,800 kJ/kWh	4,300 kJ/kWh
Roundtrip Efficiency	42%	54%

The world's first CAES plant located near Huntorf, Northern Germany has operated since 1978 with a rated power of 321MW (upgraded from 290MW in 2007) (E.ON, 2013). The Huntorf CAES plant which can generate electricity less than 3 hours was mainly built for spinning reserve for a regional nuclear plant. It is currently serving to level the variable wind turbine power (Crotogino et al., 2001; Steta, 2010; Succar, 2008). Two salt caverns with a

total volume of 310,000m^3 store compressed air at the pressure between 4.2 MPa and 7.2 MPa. The second CAES was built in McIntosh, Alabama. The McIntosh plant provides a long-term generation period of up to 26 hours due to the help of a larger cavern volume of 560,000m^3. This plant stores excess electric energy from Power South coal-fired plant and retrieves it during on-peak, high-priced times (Dresser-Rand, 2010).

Figure 2.3 illustrates the schematic diagram of the McIntosh CAES plant. The fundamental schematics for the CAES plants in Huntorf, Germany and McIntosh, AL are identical except for the recuperator, in which the waste heat of the exhausted air from a low pressure expander is recycled to increase the compressed air temperature before it goes into a high pressure combustion chamber. By making use of the recuperator, the fuel consumption of the McIntosh CAES plant was decreased by 25% relative to the Huntorf CAES plant (A. J. Pimm, 2011).

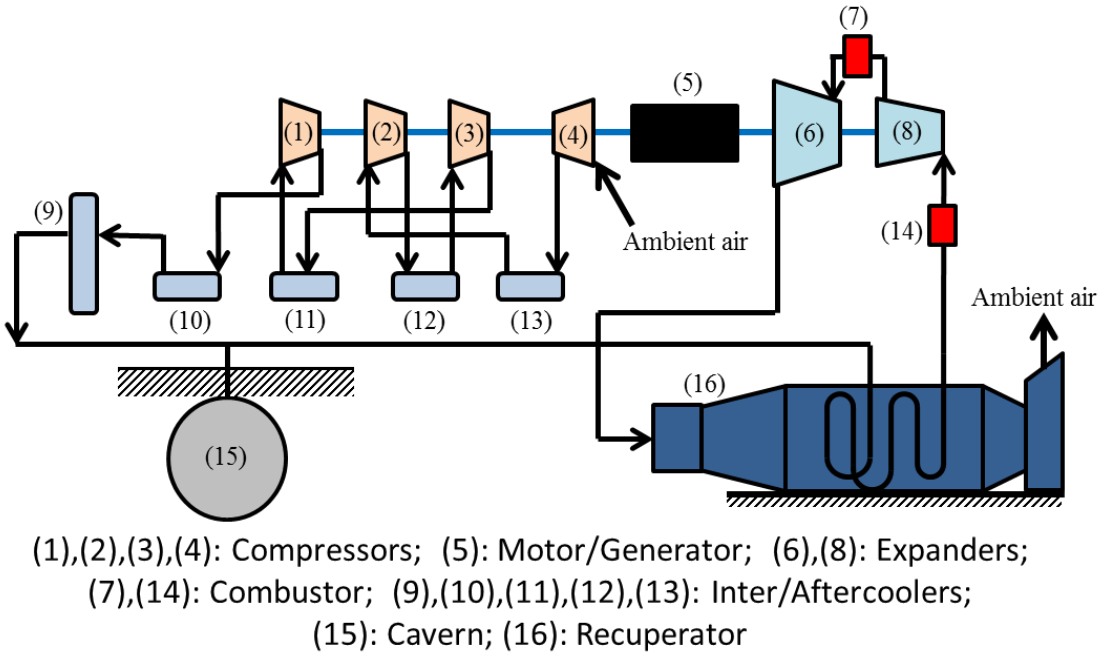

Figure 2.3 Schematic of the McIntosh CAES plant

2.3. Advanced CAES Systems

After the successful operation of the existing CAES plants with high reliability, a broad range of efforts to improve system efficiency and reduce fuel consumption has been made. While many CAES applications combined with other power systems, such as a concentrating solar thermal power generator (Garrison, Kapner, & Webber, 2009; Garrison & Webber, 2011), diesel generator (Ibrahim, Basbous, Ilinca, & Dimitrova, 2011), and biomass gasification (Denholm, 2006), have been studied, adiabatic CAES and isothermal CAES systems are mainly being investigated for utility scale CAES plants (Garrison et al., 2009; Grazzini & Milazzo, 2008; Jakiel, Zunft, & Nowi, 2007; Rice, 2011; Van de Ven & Li, 2009;

Zunft, Jakiel, Koller, & Bullough, 2006). A development research approach on turbomachinery systems for OCAES is being explored in the same way for inland CAES plants, except that the equipment must be located on a floating platform. In a conceptual design phase, turbomachinery components can be designed independently of specific storage types, although scaling and optimizing for a full system must be carried out afterward.

2.3.1. Adiabatic CAES

An adiabatic CAES system has a thermal energy storage (TES) system instead of a combustion chamber in order to increase overall efficiency by recycling compression heat. TES has been widely used in conjunction with solar energy generation since the 1980s and suitable heat storage materials such as salt or concrete are the primary materials used for TES (Hartmann, Vöhringer, Kruck, & Eltrop, 2012). In an adiabatic CAES system, heat generated during the air compression process is stored in a TES and supplied to the compressed air prior to expansion. This concept of an adiabatic CAES system with efficiencies over 70% was investigated by the EU-funded AA-CAES project for five years. Based on the result of the AA-CAES project, RWE, General Electric, Zublin AG, and the German Aerospace Center (DLR) launched the ADELE project to construct and test the world's first adiabatic CAES plant in Germany. The construction will begin in 2015 in Staßfurt, Sachsen-Anhalt, Germany (Uken, 2012).

The concept of an adiabatic CAES is considered to be the baseline of OCAES system proposed in this study, making use of existing adiabatic technologies.

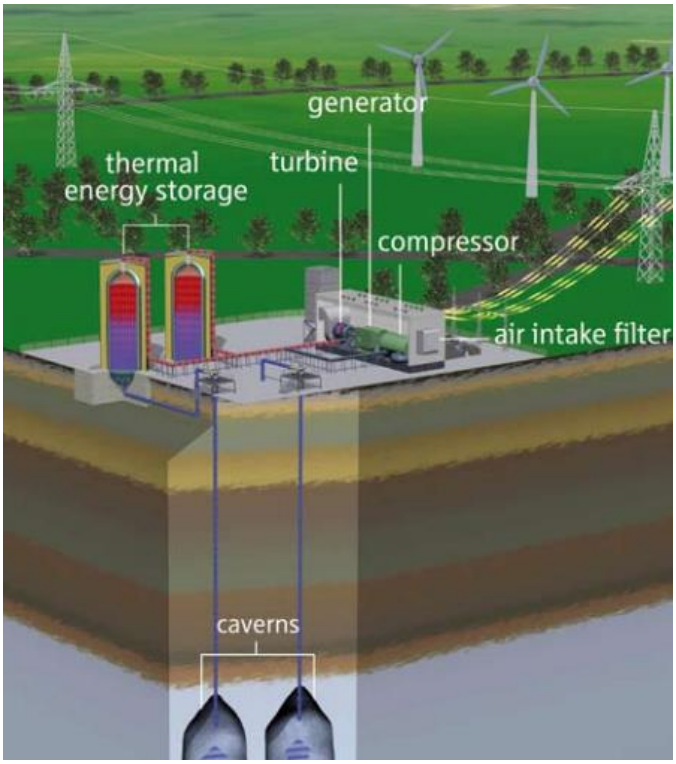

Figure 2.4 Schematic of the ADELE project

2.3.2. Isothermal CAES

Recently, isothermal compression and expansion systems for a CAES system are being developed by several companies, such as General Compression, Inc., Sustain X, Inc., and LightSail Energy, Inc. In an isothermal process, the system changes while the temperature remains constant. Isothermal compression allows air to be compressed without temperature increase; in other words, this process represents the minimum required work for the compression process. By increasing heat transfer between air and ambient 'infinite heat storage' during compression and expansion, there is no requirement for a TES, combustor, or a series of intercoolers. Various concepts for an isothermal system have been proposed: a

water spray injection, a hydraulic air compressor (Coney, 2002), a liquid flooded compressor (Hugenroth, Braun, Groll, & King, 2007), and a liquid piston (Van de Ven & Li, 2009). Some demonstration plants are under construction to test the feasibility of a utility-size system (TheEconomist, 2012). Although the overall efficiency of an isothermal CAES system is claimed to be as high as 90%, there are no industrial machines as of yet which approach these efficiency levels. The main challenges for a near-isothermal process are that it is a very slow process which requires very high heat transfer coefficients between critical components of the system. Figure 2.5 shows the concept of a liquid piston incorporated with water spraying.

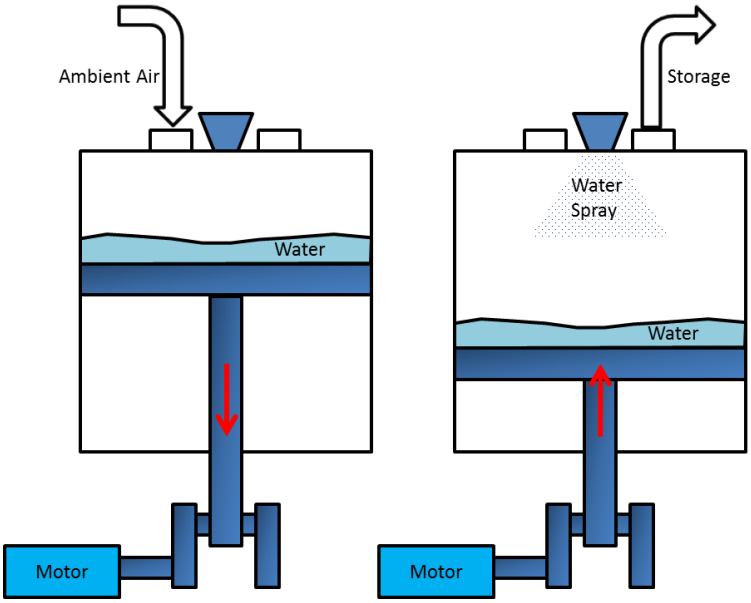

(a) Compression mode

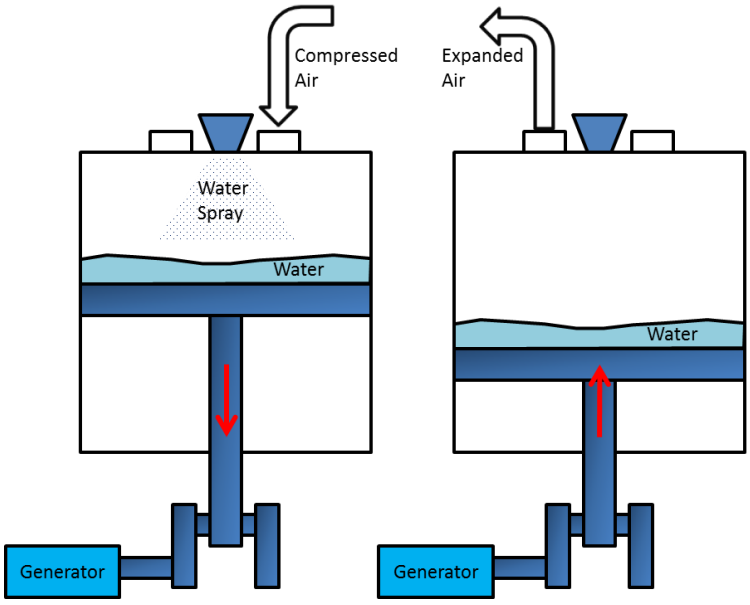

(b) Generation mode

Figure 2.5 Concept of liquid piston with water spraying

2.4. Thermodynamic Analysis of McIntosh CAES plant

The thermodynamic analysis on the McIntosh plant is carried out to evaluate the parameters, such as temperature, pressure, power rating, and efficiency, for each compression and expansion stage. The results from this analysis are used to design the subsystems of an OCAES system in the next chapter. The actual operating data of the McIntosh plant were obtained from the EPRI final report, EPRI TR-101751-V2 (Pollak, 1994b).

2.4.1. Analysis Method

For thermodynamic analysis of a CAES system, each operating stage for a compressor, an underground cavern, and a turbine in a CAES system can be analyzed separately.

Throughout the operating process of CAES, air is assumed to follow the ideal gas law, which is given by

$$P \cdot V = m \cdot R_{specific} \cdot T$$

where P is the pressure of gas, V is the volume of gas, m is the mass of gas, T is the temperature of gas and R is specific gas constant.

While air undergoes a large change in pressure between 0.1MPa to 7MPa, the compressibility factor at 293K is shown to be between ranges from 0.97 to 1 (Bejan, 2006). It can therefore be assumed that the compressed air in an underground cavern behaves like an ideal gas.

For a compressor and turbine, air is considered to undergo a polytropic process as

$$P \cdot V^n = const$$

where n is the polytropic index.

Compressor train

A compressor train consists of several compressors and intercoolers. The compressors are driven by electric motors. The compressor pressurizes ambient air and delivers it to an air storage cavern. After each adiabatic compression stage, the intercoolers dissipate heat from the compressed air in order to decrease the work required to compress the air so that the overall efficiency of CAES system can be improved. Assuming that a system operates in a steady state, the rate of work (or the power) input is defined as follows:

$$\dot{W}_{comp,in} = \frac{\dot{m}\int_{P_1}^{P_2} vdP}{\eta_{mechanical}} = \frac{\dot{m}(h_2 - h_1)}{\eta_{mechanical}} = \frac{\dot{m} \cdot \overline{C_p} \cdot (T_2 - T_1)}{\eta_{mechanical}}$$

where $\dot{W}$ is power, $\dot{m}$ is mass flow rate, h is enthalpy, $\overline{C_p}$ is average specific heat at constant pressure. The mechanical efficiency includes mechanical losses such as friction loss.

If the polytropic efficiency is given, the polytropic index can be calculated by its definition,

$$\eta_{comp,p} = \frac{\frac{k-1}{k}}{\frac{n-1}{n}}$$

$$n = \frac{1}{1-(\frac{k-1}{k\eta_{comp,p}})}$$

where n_p is the polytropic efficiency, and k is the specific heat ratio, C_p/C_v. If the input and output data of temperature and pressure are given, the polytropic index can be also obtained as follows:

$$n = \frac{\ln\left(\frac{P_2}{P_1}\right)}{\ln\left(\frac{P_2}{P_1}\cdot\frac{T_1}{T_2}\right)}$$

In the case that the initial temperature, polytropic efficiency, and pressure ratio of a compression are provided, the final temperature can be obtained as follows:

$$T_2 = T_1 \times \left(\frac{P_2}{P_1}\right)^{\frac{n-1}{n}}.$$

Turbine train

Similar to compressor trains, a turbine train has several expansion stages. The reason for this is to maximize extraction of potential energy in compressed air, resulting in increased roundtrip efficiency of the CAES system. For a steady-state and polytropic expansion process, the equation defined for the compression process can be used:

$$\dot{W}_{turb,in} = \frac{\dot{m}\int_{P_1}^{P_2} vdP}{\eta_{mechanical}} = \frac{\dot{m}(h_2 - h_1)}{\eta_{mechanical}} = \frac{\dot{m}\cdot\overline{C_p}\cdot(T_2 - T_1)}{\eta_{mechanical}}$$

A polytropic index and efficiency can be calculated if one of the following is given.

$$\eta_{turb,p} = \frac{\frac{n-1}{n}}{\frac{k-1}{k}}$$

$$n = \frac{1}{1-\eta_{turb,p}\left(\frac{k-1}{k}\right)}$$

As mentioned in the compressor train analysis, we can estimate the polytropic index in the same way when the temperatures and pressure for inlet and outlet are given. The final temperature of a polytropic expansion stage can be obtained using the equation for compression if the initial temperature, pressure ratio, or polytropic efficiency are given.

Underground cavern

Estimated energy stored into a cavern varies significantly among different expansion paths (e.g. isothermal, isentropic, and polytropic). Thus, we choose one of the following methods to calculate the potential energy in compressed air: expansion path or exergy analysis. To evaluate the energy of compressed air in an air storage system, an isothermal process is considered in this study. Work done in an isothermal process represents the minimum required work for a compression cycle or the maximum work done by compressed air without any external energy input. Using the ideal gas law, work done in a quasi-static isothermal process from condition 1 to condition 2 is defined as:

$$W_{1-2} = \int_{V_1}^{V_2} P dv = mR_{air}T_1 \ln\frac{V_2}{V_1} = P_1V_1 \ln\frac{P_1}{P_2}$$

This work is defined as work done by compressed air on the environment (i.e. a negative sign for compression and a positive sign for expansion).

In the case of conventional CAES systems with underground caverns, in which the withdrawing air undergoes a pressure change, the above equation is developed to specify the amount of actual withdrawing air as follows:

$$W_{1-2} = \left(P_1 \cdot V_{storage} \ln \frac{P_2}{P_{amb}} - P_2 \cdot V_{storage} \ln \frac{P_2}{P_{amb}} \right)$$
$$= \left(P_1 - P_2 \right) \cdot V_{storage} \cdot \ln \left(\frac{P_2}{P_{amb}} \right)$$

where subscript (1) refers to the condition of cavern fully charged with air, and subscript (2) refers to the condition of cavern reached to minimum pressure.

Efficiency

Because a CAES system operates with two different inputs, electricity and fuel, the performance of the CAES system is described by two factors, which are heat rate and energy ratio as follows:

$$Energy\_ratio = \frac{Electricity\_in}{Electricity\_out}$$
$$Heat\_rate = \frac{Fuel\_energy\_In}{Electricity\_out}$$

The overall efficiency of the CAES system is then defined by those factors as:

$$\eta_{Overall,CAES} = \frac{1}{Energy\_ratio + Heat\_rate}$$

For comparison, we refer to the definition of overall efficiency for a single-cycle gas turbine which uses only fuel energy as an input.

$$\eta_{Overall,GT} = \frac{1}{Heat\_rate}$$

2.4.2. First Law Thermodynamic Analysis

The input data and analysis results of the compressor train and the expander train are listed in Table 2.2 and Table 2.3. (All data is converted to SI units.)

Table 2.2: Input data and results of the compressor train

Compressor train, Average power mode, $\dot{m} = 89.36 kg/s$					
		1st Comp.	2nd Comp.	3rd Comp.	4th Comp.
Inlet	Pressure [MPa]	0.10	0.40	1.06	2.43
	Temperature [K]	295.37	304.82	304.82	304.82
Outlet	Pressure [MPa]	0.41	1.07	2.45	6.27
	Temperature [K]	459.82	424.48	407.04	423.43
Results	Polytropic efficiency	0.9097	0.835	0.825	0.815
	Power input [MW]	15.25	11.09	9.48	11.00

From the result, the total required power for the compressor train is 46.81 MW which is regarded as input shaft power. From the data sheets, the rated electrical power input to the compressor train is 49 MW. Therefore, the electrical motor efficiency of the compressor train can be evaluated to be 0.955.

Table 2.3: Input data and results of the turbine train

Expander train, Average power mode, $\dot{m} = 156.95 kg/s$						
		Recup.	1st CC	HPT	2nd CC	LPT
Inlet	Pressure [MPa]	4.48	4.35	4.31	16.27	15.17
	Temperature [K]	308.15	559.04	810.93	653.71	1144.26
Outlet	Pressure [MPa]	4.35	-	1.63	-	0.10
	Temperature [K]	559.04	810.93	653.71	1144.26	641.48
Results	Polytropic efficiency	-	-	0.7745	-	0.7574
	Power output [MW]	-	-	26.77	-	87.59

The estimated shaft power output is 114.36 MW from the result and the rated electrical power output from the expander train is given in the data as 110W. Thus, the electrical generator efficiency of the expander train is estimated to be 0.962.

The parameters to evaluate an overall efficiency of the system have been also given in the operating data sheet. Having the given heat rate, 1.2087 [MWh/MWh], and the electrical input and output powers at rated load, the overall efficiency of the McIntosh CAES plant is calculated as follows:

$$\eta_{Overall,CAES} = \frac{1}{Energy\_ratio + Heat\_rate}$$
$$= \frac{1}{\frac{49MW \times 41hr}{110MW \times 26hr} + 1.2087}$$
$$= 0.523$$

Despite the fact that the nominal powers of the McIntosh CAES plant are given in the EPRI final report, our energy flow analysis presents end-to-end calculations for the system which includes the efficiencies of the compressor and turbine trains.

2.5 Conclusions

In this chapter, we introduced the concept of compressed air energy storage (CAES) system and presented advanced CAES systems. In order to get more details of operating conditions in the McIntosh CAES plant, the first law analysis was conducted for the overall configuration. Based on the given data, we were able to find the polytropic efficiencies and motor/generator efficiencies of each compressor and turbine component. These data will be used to design the system configuration of ocean compressed air energy storage (OCAES) in the next chapter which will have different pressure ratios and power capacities from the existing CAES plants.

With regard to the conversion efficiency of fossil-fuel resources, we can also find that the overall efficiency of the existing CAES plant, 52.3%, is competitive to that of a combined cycle gas turbine which is claimed to have the overall efficiency as high as 60%. If we presume the electricity input to the CAES system is “to-be-wasted” so it is a free energy, the energy conversion efficiency regarding fossil fuels is to be 74.7%.

CHAPTER 3

OCEAN COMPRESSED AIR ENERGY STORAGE

3.1. Background

The basic concepts of an OCAES system were introduced in the papers written by Seymour (Seymour, 1997, 2007). In these papers, an OCAES is described as a modified CAES system which is a promising alternative when an underground cavern is not available. While the existing CAES plants employ underground salt caverns, an OCAES system would make use of an 'underwater' structure for air storage. The air chamber, to be installed on the sea-floor, can be an open-ended reservoir or a flexible bladder. Compressed air delivered to the underwater air container will displace seawater and due to the hydrostatic pressure at a particular water depth, the compressed air will be maintained at a constant pressure. The hydrostatic pressure increases approximately by one tenth of a megapascal for every ten meters of water depth. Thus, water depths of 600m is required to design an OCAES system with 6 MPa in gauge pressure, for example. The Seymour papers present an overview of OCAES systems, and introduce two possible designs of an air chamber. In "Undersea Pumped Storage for Load Leveling" (Seymour, 1997), an OCAES system is presented which would have a 230MW capacity for 10 hours a day; this system would utilize compressed air kept at 6 MPa contained in a pipe in which the diameter and length are 3.6m and 12.8km, respectively. Another approach, outlined in "Ocean Energy On-demand Using Underocean Compressed Air Storage" (Seymour, 2007), utilized an air containment structure with a

ballast bin. The paper presents calculations which show that the tank, which is 30m wide, 8m high, and 300m in length at a depth of 650m, would contain enough compressed air to produce 1GWhr of electricity. After reviewing these papers, it became clear that the concept of OCAES systems integrated with offshore renewable energy brings significant benefits, especially on the North Carolina coast and along the southern east coast of the United States. In this chapter, the conceptual design of overall OCAES system is presented along with advantages over existing CAES systems, geographical discussion in North Carolina, and design candidates for an underwater air container.

3.2. Offshore Renewable Energy

As worldwide public concerns about the limited reserve of fossil fuel along with the environmental impact of global warming are looming large, the demand of renewable energy generation is significantly growing in recent years. In addition to inland wind and solar resources, the development of offshore renewable energy is undergoing rapidly. Offshore energy production shows great promise, because the energy density of wind energy is much larger and more consistent in offshore areas. According to the National Renewable Energy Laboratory (NREL), the potential generating capacity from the United States offshore winds is estimated to be more than four times the current electric capacity of the United States. Offshore wind projects of more than 2,000 MW of capacity are being planned in the United States, and the first offshore wind farm of the United States, called the “Cape Wind Project”, has been recently approved after a lengthy permitting process (Eilperin, 2010; Musial & Ram, 2010). Maximum capacity of this wind farm is expected to be 454 MW from 130 wind

turbines. In addition, the Gulf Stream along the east coast of the United States is another energy source, which is 25 to 80 km away from the North Carolina coastline. Additionally, the peak surface speed of the Gulf Stream is over 2.5 m/s (Adams, 1999).

3.3. North Carolina Geographical Discussion

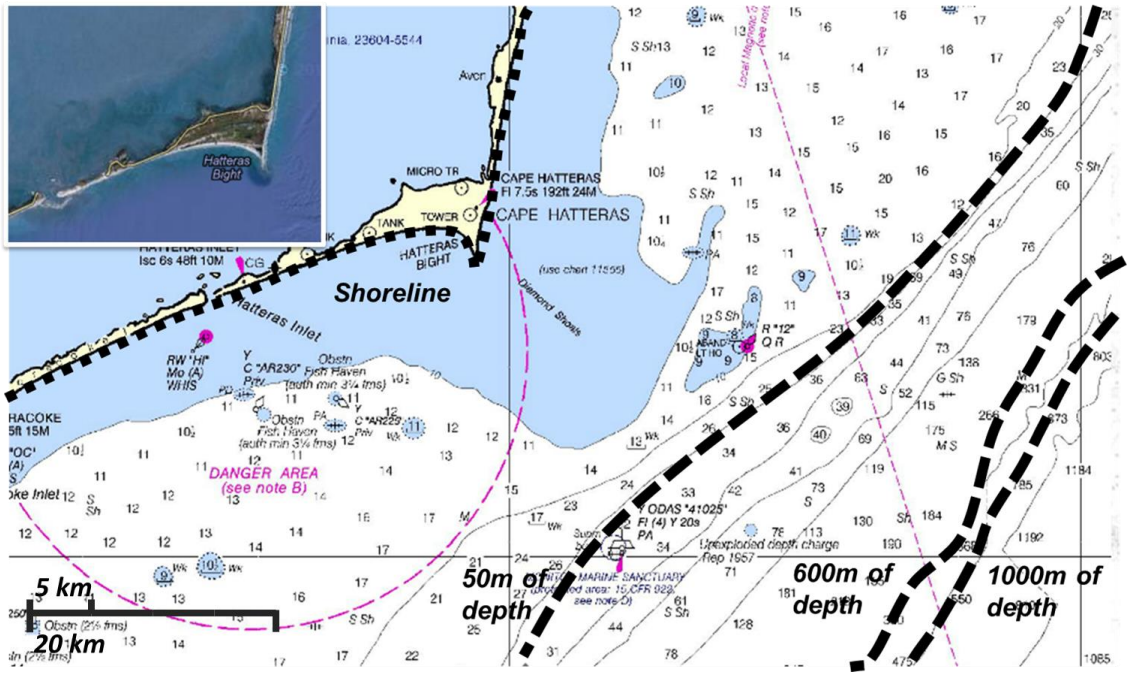

Figure 3.1 Bathymetric map of the coast of Cape Hatteras (units in fathom)

Figure 3.1 is the bathymetric map of the NC coast (NOAA, 2011). It is relatively difficult to find deep water regions (300m ~ 600m depths) for OCAES along the NC coastline compared to the Pacific coast of the U.S. where 600m depths can be found, in some places, 3km away from the coastline (e.g. Lopez point, CA). However when the OCAES system works in

collaboration with offshore renewable energy sources, the geographic characteristics of the NC offshore become more beneficial to our OCAES system designs. As shown in Figure 3.1, the water depth is increasing gradually up to 40km off the coast of Cape Hatteras. And the area between 40km and 70km off the coast includes a rapid change in water depths from 50m to 1000m. A wind turbine, which is currently the most feasible option for renewable energy generation in an offshore area, can be safely installed in up to 30m water depth with a monopole foundation design (Milborrow, 2003). Offshore wind turbines in deep water with depths of over 30m require more complex and expensive foundation systems that are tripod, or four-legged, and involve truss foundations, which require high installation costs and significant R&D efforts (Musial & Butterfield, 2004; Nikolaos, 2004).

Strong wind is available in the areas around 40km off the coast and a well-proven simple monopole foundation technology is feasible in water depths of less than 30m. Moreover since the Gulf Stream overlaps this area, it should be possible to harvest both wind and marine current energy in this area. The length of outfall pipes from a platform to an air chamber at the depth of 600m would be less than 30km in the horizontal direction if the platform is located between the renewable energy farms and the air storage container. The electric power can then be transmitted to an electrical distribution grid via high-voltage underwater cables. Based on these characteristics of both OCAES and offshore wind turbine locations, the North Carolina offshore geography presents a feasible OCAES system location.

3.4. Benefits of OCAES

OCAES has advantages over underground CAES in energy availability. As OCAES stores compressed air underwater, the hydrostatic pressure allows for the holding and dispatching of the air at a constant pressure. In existing CAES systems, compressed air is throttled from 7 MPa to 4.5 MPa, with substantial energy losses, to allow turbines to operate at a highly desirable fixed inlet pressure. Adjustment of air pressure through throttling is not necessary in OCAES system, thus the system more efficiently extracts the energy from the high pressure of the compressed air.

A comparison of the specific energy before and after throttling will help to determine the energy loss. As mentioned in the previous chapter, work done by compressed air is varied widely depending on an expansion process. In order to investigate the potential energy in compressed air, it can be assumed that compressed air expands isothermally. The equation for work done in a quasi-static isothermal process from condition 1 to condition 2 is recalled as:

$$W_{1-2} = mR_{air}T_1 \ln \frac{P_1}{P_2}$$

Dividing the isothermal work by the mass of compressed air, the specific energy is then described as:

$$w_{1-2} = \frac{W_{1-2}}{m} = R_{air}T \ln \frac{P_1}{P_2}$$

The cavern pressure change of a CAES system is considered from 7 MPa to 4.5 MPa assuming a linear decrease in pressure drop with respect to time. While the net specific

energy of compressed air remains constant due to regulated air pressure, the gross specific energy decreases as the cavern pressure is changing.

In Figure 3.2, the blue line represents the gross specific energy and the red line represents the net specific energy. The gap between the blue and red lines shows the energy loss due to throttling. The dissipated energy due to throttling throughout the discharging cycle is estimated about 6.2 % of the total isothermal energy in the compressed air.

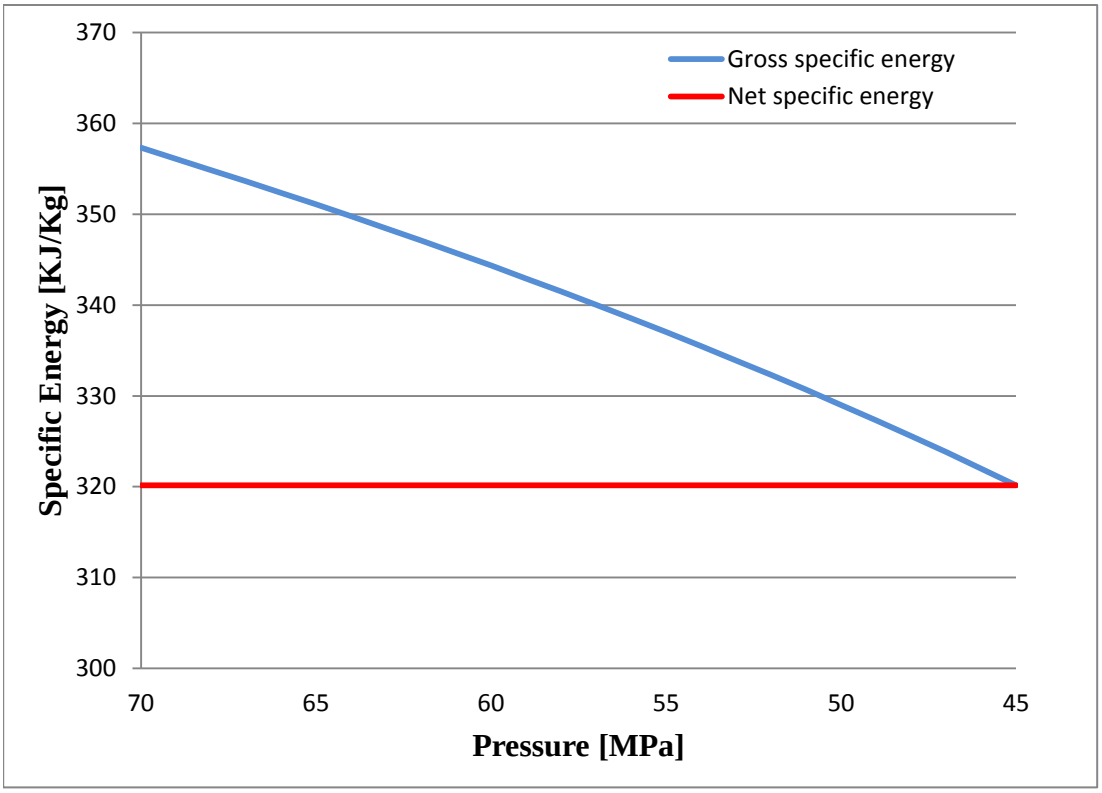

Figure 3.2 Comparison of specific energy of compressed air

Furthermore, the proposed OCAES system has the great advantage of a small storage volume compared to an underground cavern. The fixed volume of an underground cavern

must operate over a wide range of pressures (i.e. from 7 MPa to 4.5 MPa). After the air pressure of the cavern drops below the minimum required pressure (i.e. 4.5 MPa), the compressed air in the cavern is unusable. In an OCAES system, the pressure in the air chamber is always constant so that the compressed air energy stored in the chamber can be fully extracted. For calculation of the energy density of compressed air, we recall the assumptions that compressed air expands isothermally and follows the ideal gas law.

From the equation for the work involved in an isothermal expansion, the energy density of compressed air for an OCAES can be estimated by simply dividing isothermal expansion work by the volume of air storage that we have

$$\frac{W_{1-2}}{V_{storage}} = P_1 \ln \frac{P_1}{P_{amb}}$$

where P_1 is pressure of compressed air and $V_{storage}$ is volume of a storage container.

For the underground caverns of the McIntosh, AL plant, the air pressure in the underground cavern changes significantly and compressed air below 4.5 MPa is not used for power generation. Thus, recalling the work equation from section 2.4.1, the energy density of compressed air for an underground CAES can be measured as follows:

$$\frac{W_{1-2}}{V_{storage}} = \left(P_1 - P_2\right) \cdot \ln\left(\frac{P_2}{P_{amb}}\right)$$

If we consider extractable energy (recall that once the cavern pressure drops below 4.5 MPa, no more energy can be extracted), the energy density of the underground reservoir of McIntosh plant is estimated to be 2.6435 kWhr/m^3. For the underwater storage of our OCAES system, if it is filled with compressed air at the ocean depth of 450m (equivalent to

hydrostatic pressure of 4.5MPa) and the air expands to the ambient pressure, the energy density is simply calculated as 4.7583 kWhr/m^3.

3.5 Underwater Air Storage Containers

Underwater air storage containers can be designed in two different ways. Firstly, Energy bags, which have been under development at the University of Nottingham, are flexible fabric structures(i.e. flexible bladders) that store compressed air at the hydrostatic pressure in a water column as they inflate like a balloon (A. Pimm & Garvey, 2009; A. J. Pimm, 2011). Prof. Garvey has, however, recently indicated that inflatable bags are no longer considered the best solution (Seymour, 2012). Another balloon-shaped flexible accumulator is under development at the University of Windsor in conjunction with the energy company Hydrostor, and they recently demonstrated the behavior of the pilot accumulator, along with the air charging and discharging processes, in Lake Ontario (Cheung, 2012). Secondly, an open-ended containment structure made of steel or concrete can be a possible air storage device for OCAES systems: stacked pipes and a rectangular tank. While the flexible bladder only contains compressed air, the open-ended structure is filled with compressed air and/or water. The actual shapes of air storage designs will be determined by economic concerns and installation feasibility due to the corrosive environment of seawater. Figure 3.3 shows various types of underwater containers (A. J. Pimm, 2011; Seymour, 2007).

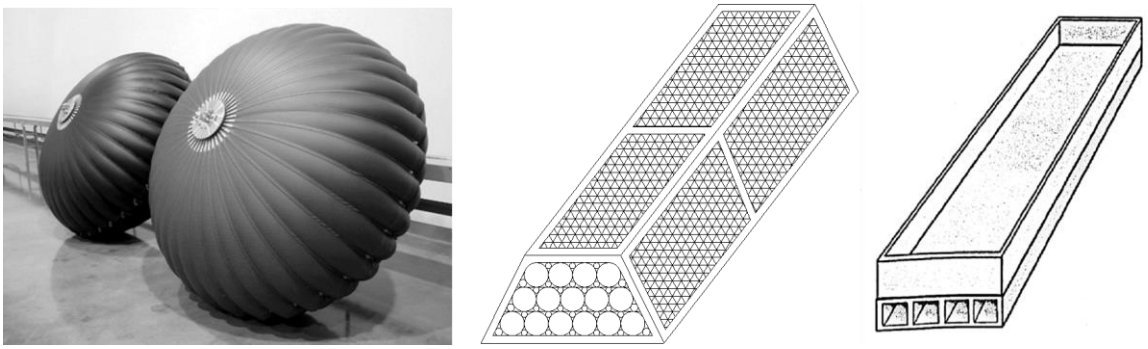

Figure 3.3 Prototype of the Energy bag, schematic of stacked pipe model and air containment structure (from left)

Decommissioned oil tankers and submarines were also examined due to their large internal volume and the reduced time and cost of fabrication. However these plans were discarded because environment issues associated with PCBs (polychlorinated biphenyls) came up during installation of an existing artificial reef using a decommissioned ship in Florida (Self, 2011). PCBs were used widely in paints, cements, PVC coatings, retardants, sealants and so on before being banned by the United States Congress in 1979. PCBs are known to cause cancer and serious effects on the immune system, reproductive system, nervous system, and endocrine system. According to data from the study by the Florida Fish and Wildlife Conservation Commission (FWC), total PCB concentrations in fish increased by 1,446% at the Ex-USS ORISKANY site after the ship was sunk (Self, 2011).

3.6 Conclusion

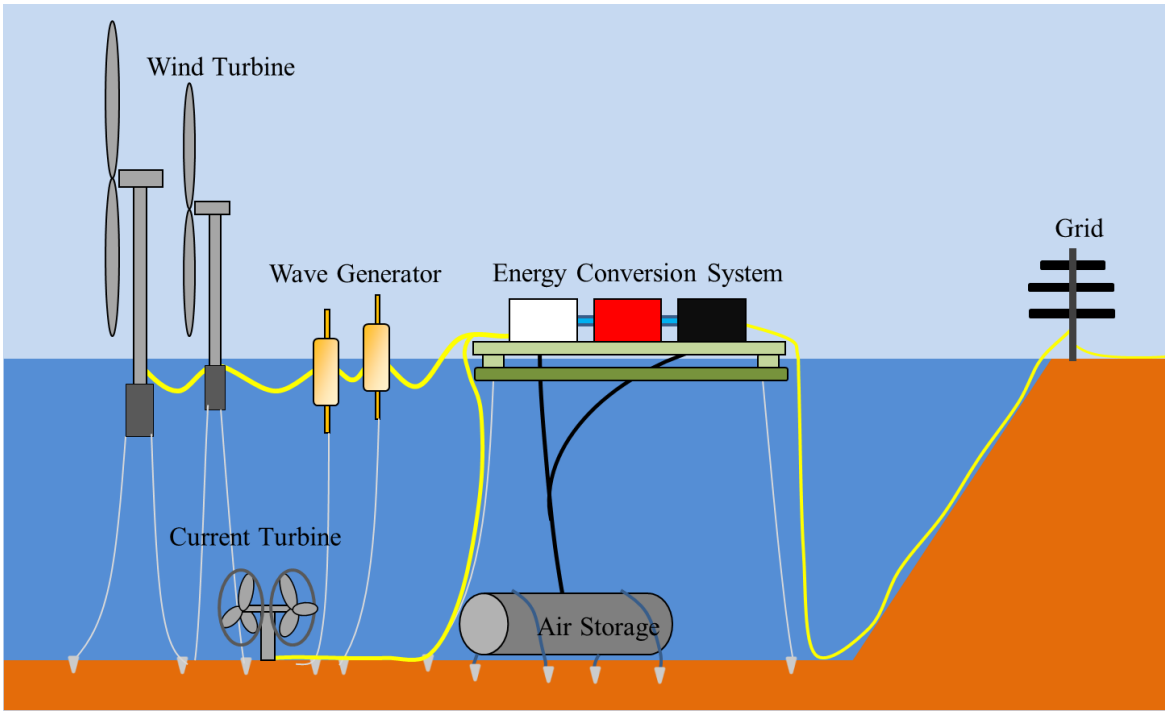

Figure 3.4 Concept of ocean compressed air energy storage system

In this chapter, we proposed a new concept of ocean-based CAES which is shown as Figure 3.4. The strong and constant offshore renewable energy sources can be harvested and utilized efficiently by incorporating CAES technologies. For the site selection of OCAES, geographical characteristics in North Carolina were discussed with the available renewable energy sources. Moreover, OCAES system is determined to have advantages because it makes use of the hydrostatic pressure of sea water to maintain the pressure of compressed air. The constant pressure of compressed air enables the removal of a throttle process in the CAES system which regulates the varying air pressure from an underground cavern. And by removing the throttling, 6.2% of required isothermal energy in compressed air is estimated to

be saved during a compression phase. Another benefit of OCAES is high energy density in an air storage container. According to the calculations of isothermal energy density within an underwater air container (when installed in water depth of 450m) and underground cavern (the pressure range from 7.0MPa to 4.5MPa), the energy density of the underwater air container is 80 percent higher than that of the underground cavern.

Lastly, to employ a CAES system to offshore renewable energy resources, the several types of underwater air storage containers were discussed. The structure made of concrete is currently being considered due to its low cost and simple fabrication.

CHAPTER 4

THERMODYNAMIC MODEL OF ADIABATIC OCAES

4.1 Introduction

In this chapter, the thermodynamic modeling of an OCAES, at a depth of 600m, is developed and analyzed based on the conceptual design proposed in Chapter 3. As discussed in Section 2.4, there are two developing advanced technologies to be used for a CAES system: adiabatic and isothermal systems. The baseline of our OCAES model makes use of adiabatic technology due to the challenges and uncertainties associated with the isothermal systems currently under investigation. The turbomachinery data of the existing McIntosh CAES system which has been successfully operated over several decades is used to conservatively examine the performance of an OCAES and a thermal energy storage (TES). The function of a TES is to store heat energy and deliver it to compressed air during an expansion, while a diabatic CAES system employs intercoolers to discharge the heat generated from compression. An adiabatic OCAES system can, therefore, avoid using fossil fuel to provide heat to the compressed air prior to expansion cycles.

The results of this thermodynamic analysis enable us to compare its energy flows to the energy flows of the existing system and to validate the feasibility of the overall system.

4.2 System Modeling

The simplified thermodynamics model of an adiabatic OCAES system is based on the data from the McIntosh, AL plant (Pollak, 1994a, 1994b) and TES systems in solar power plants (Gil et al., 2010; Medrano, Gil, Martorell, Potau, & Cabeza, 2010). The structure of the model includes a three-staged compressor train, a thermal energy storage, an air reservoir, and a three-staged expander train. Figure 4.1 shows the schematic of adiabatic OCAES system.

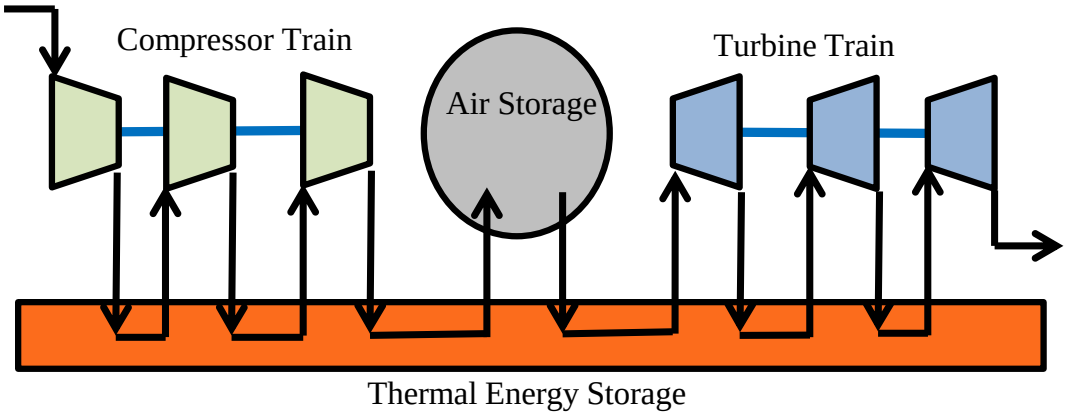

Figure 4.1 Adiabatic CAES schematic diagram

4.2.1 Compressor Train

An electric-driven compressor train consists of one axial stage and two centrifugal stages. We modified the mass flow rate and pressure ratios of the OCAES compressor train, the polytropic efficiency and motor/generator efficiency are directly taken from the analysis data of the McIntosh plant's compressor train. In thermodynamic aspects, polytropic efficiency is

defined independent of the temperature and pressure of air being compressed while adiabatic efficiency is defined dependent on pressure ratios of the air (McAllister, 2009). Between each stage in the train, heat exchangers are placed to capture compression heat. Heat transfer fluid (HTF) may be different depending on the types of TES systems. For example, thermal oil may be used to transfer heat energy from compressed air to a TES indirectly through heat exchangers. In another way, high temperature compressed air may be directly working as HTF. For an OCAES system, using compressed air as HTF would be desirable since it requires less complicated heat-transfer processes lowering installation costs. In addition, the train may be in need of an aftercooler behind a heat store process in order to increase the compressor efficiency by lowering air temperature to the ambient temperature.

4.2.2 Turbine Train

The turbine train for an OCAES has three stage expanders, which is modified from the existing CAES system because of high pressure of air and the limit of the inlet temperature of the air. Besides the fact that the air pressure supplied to the turbine is kept at 6 MPa, the temperature of a TES is restricted by the maximum temperature from compression cycles as well. Therefore, the turbine is divided into three stages with respect to acceptable pressure and temperature drops, avoiding of exhaust.

4.2.3 Thermal Energy Storage

Thermal energy storage is the most critical subsystem in our adiabatic OCAES system. Heat energy produced during compression cycles is stored in a TES and compressed air from an

underwater air container passes through the TES to be heated before entering to each turbine stage.

The heat storage materials selected for this study are high temperature concrete and Solar salt. As an attractive candidate for a sensible heat storage material, high temperature concrete has been investigated by the German Aerospace Center (DLR). According to their studies, the high temperature concrete appears suitable for heat storage mediums by reason of low costs, easy handling, and high structural stability (D. Laing, Lehmann, D., Fiss, M., & Bahl, C., 2009; D. Laing, Steinmann, W. D., Tamme, R., & Richter, C., 2006).

Another heat storage material is Solar salt (60% $NaNO_3$ + 40% KNO_3). There are two well-known candidates of molten salt for TES, which are Solar salt and Hitec XL (48% $Ca(NO_3)_2$ + 7% $NaNO_3$ + 45% KNO_3). In the case of solar power generating systems, molten salt is normally acting as both heat transfer and heat storage mediums. Therefore, the important factor to decide a type of salt is low freezing temperature which helps to reduce maintenance costs preventing freezing of the salt. Since Hitec XL freezes at 142˚C which is lower than 220˚C, the freezing point of Solar salt, Hitec XL is more desirable salt for the TES of solar power plants. On the other hand, compressed air is acting as the heat transfer medium in our OCAES system and the molten salt would be isolated in the TES serving as a passive thermal storage material. Since the salt used in the OCAES system is not necessarily kept in a molten state, Solar salt is preferable due to its lower cost than Hitec XL. The characteristics of high temperature concrete and Solar salt are shown in Table 4.1 (Gil et al., 2010; Kearney, 2003; D. Laing, Steinmann, W. D., Tamme, R., & Richter, C., 2006).

Table 4.1: Specifications of thermal storage materials

	Unit	High temperature concrete at 350˚C	Solar salt at 300˚C
Density	kg/m^3	2750	1899
Specific heat capacity	kJ/kg-K	0.916	1.495
Thermal conductivity	W/m-K	1.0	0.5

4.2.4 Underwater Air Storage Container

In this chapter, the type of air storage system is not specified. Yet the size and number of volume of underwater air storage units will be estimated based on thermodynamic analysis of the turbomachinery systems.

4.2.5 Summary of Operating System Requirements

Table 4.2 presents the fundamental parameters for the system model.

Table 4.2: Design parameters for an OCAES model

	Unit	Parameter
Air storage		
Installation depth	m	600
Absolute pressure	MPa	6.134
Compressor		
Mass flow rate	kg/s	100
Operating time	hour	15
Configuration		Three stages: Axial, Centrifugal, Centrifugal
Pressure	MPa	0.1 - 0.7 - 2.1 - 6.3
Polytropic efficiency		0.91, 0.82, 0.82
Elec. motor efficiency		0.955
Turbine		
Mass flow rate	kg/s	150
Operating time	hour	10
Configuration		Three stages : High, Mid, Low
Pressure	MPa	6 - 1.5 - 0.5 - 0.1
Polytropic efficiency		0.8, 0.8, 0.8
Elec. generator efficiency		0.962

4.3 Analysis Method

4.3.1 Compressor Train / Turbine Train / Underwater Air Storage

The compressor and turbine trains are following polytropic process which has introduced in section 2.4.1. Therefore, the performance of the compressor and turbine trains of OCAES are evaluated in the same way except for the adjustments of pressure ratios and mass flow rates.

For the underwater air storage system, there is no need to determine its potential energy at this point. Since, however, the volume of the storage system is dependent on the power

capacity of compressor and turbine systems, the volume can be determined by the design parameters of an OCAES model. The volume of an air container is estimated by the ideal gas law with the mass flow rate and operating hours of the compressor train as follows:

$$V_{storage} = \frac{m \cdot R_{air} \cdot T}{P} = \frac{\dot{m}_{comp} \cdot t}{\rho_{air}}$$

where m is total mass of air in underwater air storage, $\dot{m}_{comp}$ is mass flow rate of the compressor train, t is charging time, T is water temperature at 600m below sea level, P is hydrostatic pressure at 600m below sea level.

4.3.2 Thermal Energy Storage

Both Solar salt and high temperature concrete are classified as sensible heat storage materials. Sensible heat is associated with the change in temperature of the material while thermal energy is transferred. The thermal energy, Q, stored as sensible heat in material of mass, m, and specific heat, C_p, with change in temperature of the material, T_2-T_1, is defined as follows (Bejan, 2006):

$$Q = \int_{T_1}^{T_2} mC_p dT = \rho \cdot \bar{C}_p \cdot V \cdot (T_2 - T_1)$$

where $\bar{C}_p$ is average specific heat at constant pressure, V is volume of storage material.

There are more design parameters of TES systems such as thermal conductivity, diffusivity, corrosivity, and temperature range. However, considering that Solar salt has been used in solar power systems and that high temperature concrete is under research for TES, it is reasonable to assume those design factors are acceptable.

4.3.3 Efficiency

Unlike a conventional CAES system, there is one energy source, which is electricity from offshore renewables. Hence, the overall efficiency of the OCAES system can be simply determined by energy ratio (see Section 2.4.1) as follows:

$$\eta_{Overall,OCAES} = \frac{1}{Energy\_ratio}$$

4.4 First Law Thermodynamic Analysis

The first law thermodynamic analysis for the adiabatic OCAES is conducted. The shaft power input to the compressor train during charging cycle is 54.06 MW for 15 hours to fill the container. The shaft power output from the turbine train is estimated 51.81 MW for 10 hours. The details are presented in Figure 4.2 and Figure 4.3.

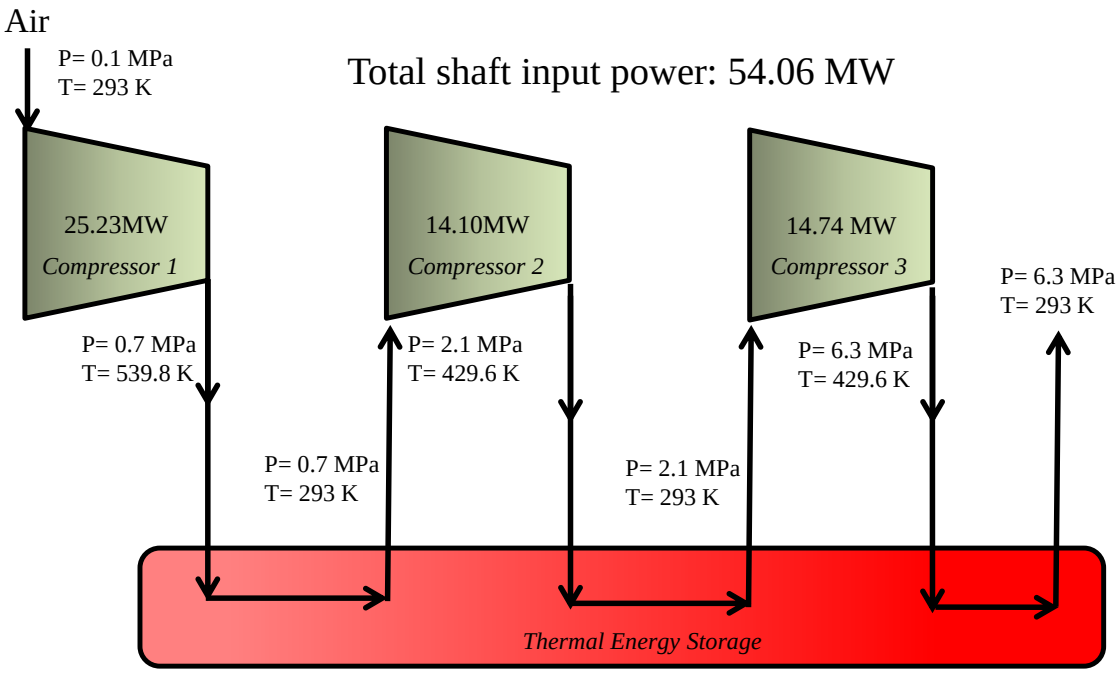

Figure 4.2 Compression processes of three-staged compressor and thermal energy storage

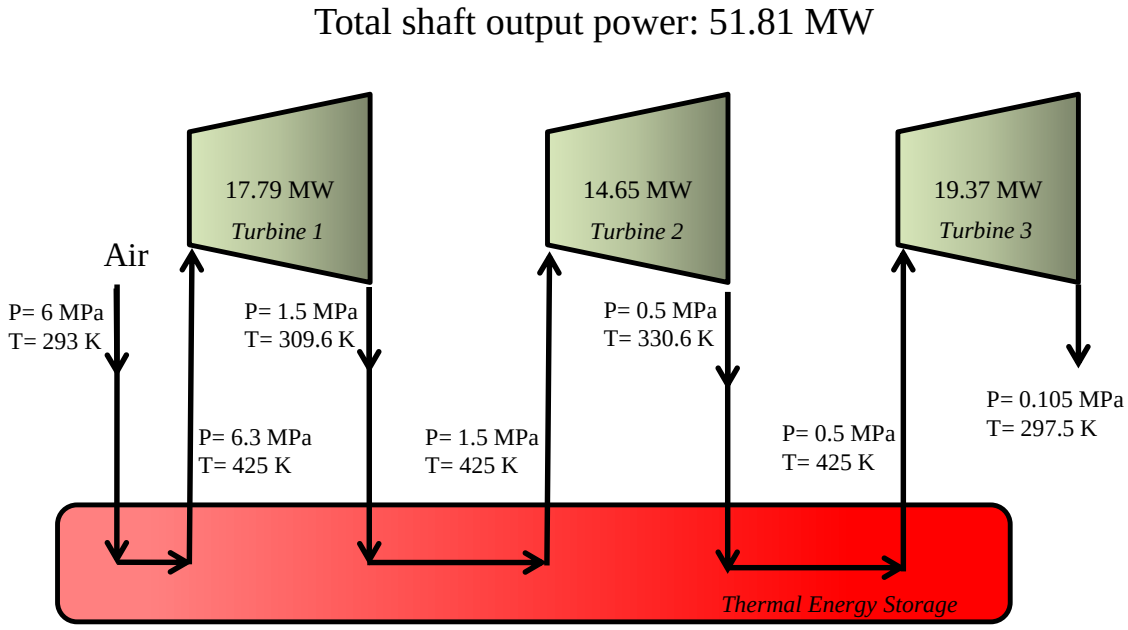

Figure 4.3 Expansion processes of three-staged turbine and thermal energy storage

All cycles are in steady state at maximum power during the each process. For the compression process, the total electric power input is 56.61 MW that is estimated by multiplying the total shaft power input by the electrical motor efficiency estimated in Chapter 3, and it is the same calculation procedure for the electric power output of the turbine train that is 49.84 MW. Therefore the overall efficiency of the adiabatic OCAES is evaluated to be 58.7%.

For our analysis, the McIntosh CAES plant is considered as a reference plant model, which is built in 1991. To be conservative, the polytropic efficiency and the electrical motor/generator efficiency of the McIntosh plant were used to our analysis. Therefore it is

expected that the overall efficiency of an adiabatic OCAES will be better than 58.7% in case that updating turbomachinery systems are engaged.

Thermal energy storage

For thermal energy, it is needed to note that the energy amount (e.g. MWhr) is not only a design factor but also the maximum temperature of energy source is a significant factor to the TES design. For example, even if there is an energy storage that can supply thermal energy for 10 hours at 100˚C, it is not sufficient even for 1 hour when a system requires 200˚C. Thus, it is a restriction to TES that the maximum temperature of compressed air after compression cycles determines the storage temperature. According to the analysis, the required thermal energy to heat compressed air before turbine cycles is evaluated to be 46.10 MW for 10 hours (461.0 MWhr), which is 56.8% of the thermal energy discharged from the compression cycles, that is 54.06 MW for 15 hours (811.0 MWhr). Based on the densities of high temperature concrete and Solar salt, the volume of TES should at least be 4990.7 m^3 and 4428.2 m^3 for high temperature concrete and Solar salt, respectively. It also should be noted that the volume of TES would be larger than the required volume due to the additional thermal energy loss associated with heat transfer processes, standby modes.

Air storage container

As the mass flow rate of a compressor train decides a system power capacity, the interior volume of an air storage container determines an operating time of both the compressor and turbine trains. Assuming no leaking and steady-state operations for the compressor train, the

total mass of compressed air to be filled in the air storage container is estimated to be 5,400,000 kg based on the given mass flow rate and operating time. Using the ideal gas law to relate the density of air to the hydrostatic pressure, the required volume of air storage is 74023.2 m^3 for our OCAES system. In the case of using a concrete storage designed by Department of Civil, Construction, and Environmental Engineering (CCEE) at North Carolina State University, which will be introduced in the next chapter, at least 82 units of the container are required for this OCAES system.

4.5 Conclusions

The first law model of the adiabatic OCAES system of which the air storage container is installed in water depth of 600m has developed. The compressor and turbine trains are designed following the specifications in the McIntosh CAES plant and the pressure ratios are modified. Since the pressure ratios and inlet temperatures are different, the polytropic efficiency obtained from the previous chapter is used for the OCAES model.

The thermodynamic parameters, such as temperature and pressure, of the OCAES system for each compression and turbine stage can be estimated through our analysis. For incorporating TES into a CAES system, the maximum temperature occurred in a compressor train is of critical importance to the power output during expansion because the maximum temperature supplied to compressed air limits the expansion pressure ratio of the compressed air before freezing. There are other restrictions of the OCAES system; sizes of a TES and an air storage container. From the results, the volumes of TES are estimated to be at least 4990.7 m^3 and 4428.2 m^3 for high temperature concrete and solar salts, respectively. And it is also

calculated that the volume of underwater air storages is 74023.2 m^3. Because an OCAES system should be located on an offshore platform to be integrated with offshore renewable energy sources, the size of TES will have to be compromised with the power capacity of the OCAES system. Considering the large size of air storage container, installation cost study will be required to verify the feasibility of actual system construction.

CHAPTER 5

MODELING OF FLOW INDUCED LOADS ON AIR STORAGE CONTAINER DUE TO OCEAN CURRENTS

5.1. Motivation

An underwater air storage structure is one of the major subsystems of an ocean compressed air energy storage (OCAES) system bringing better storage efficiency than existing underground caverns. As stated in the North Carolina geographic discussion in the previous chapter, the candidate locations for OCAES systems in North Carolina are around 40 to 70km off the coast of Cape Hatteras (where the Gulf Stream overlaps spatially). This location contains a narrowing of the Gulf Stream that produces its second fastest flow, exceeded only by its world record setting value off the coast of Miami to the south. It is also struck by tropical storms or hurricanes at least once every two years (Keim, Muller, & Stone, 2007). Thus, the loads exerted on an air storage container by ocean currents and the loads experienced by an air storage container on the ocean floor under such conditions have been evaluated by finite element analysis in order to aid in the design of anchoring and mooring systems for the container.

5.2. Air Storage Model

The air storage model shown in Figure 5.1, designed by Department of CCEE at North Carolina State University, has been examined. The model is a square frustum shape made of

concrete. This air storage model will involve an interior volume of 903m^3 which, at a depth of 300m, will be able to store 2.56 MWhr of energy in the form of compressed air via an isothermal process. We make the assumption that the dry weight of the storage structure should be at least ten times the buoyant force resulting from filling the structure with air.

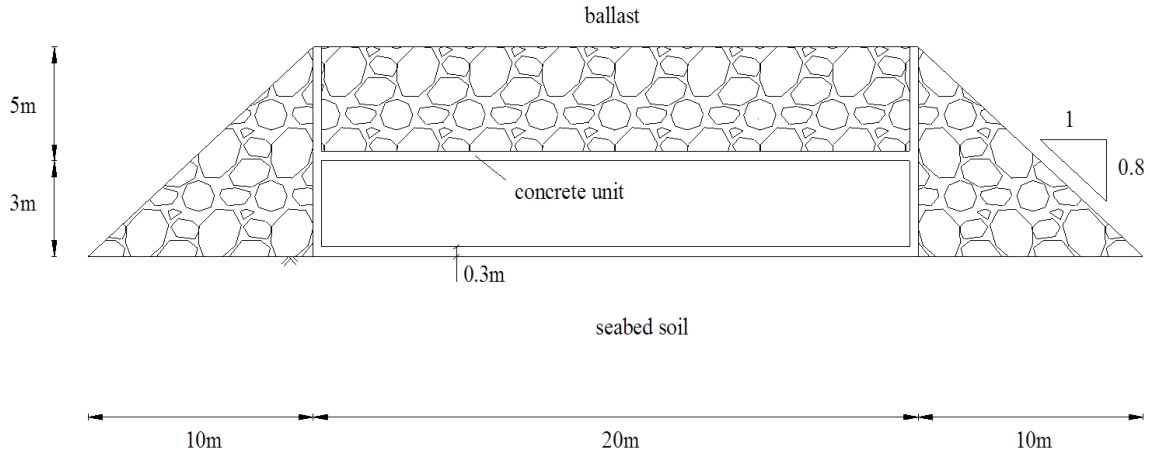

Figure 5.1 A conceptual design of air storage for OCAES by the department of CCEE at North Carolina State University

5.3. Settings

The finite element analysis of the air storage container is conducted using COMSOL Multiphysics engineering simulation software 4.3a. Turbulent Flow (RANS k-ε model) and Solid Mechanics modules are employed to examine the loads on the surface of the storage structure and the loads on the seafloor during the ocean currents are passing over the structure. In this simulation analysis, ocean currents are regarded as single direction turbulent flows with three different current velocities, 0.1, 1, and 10m/s. The flows parallel and

diagonal to the structure are evaluated. The absolute pressure is set to 3 MPa as the actual container is suggested to be located on the seabed at a water depth of 300m. The Figure 5.2 presents the flow direction setups in the air storage system: (a) Parallel current direction, (b) Diagonal current direction.

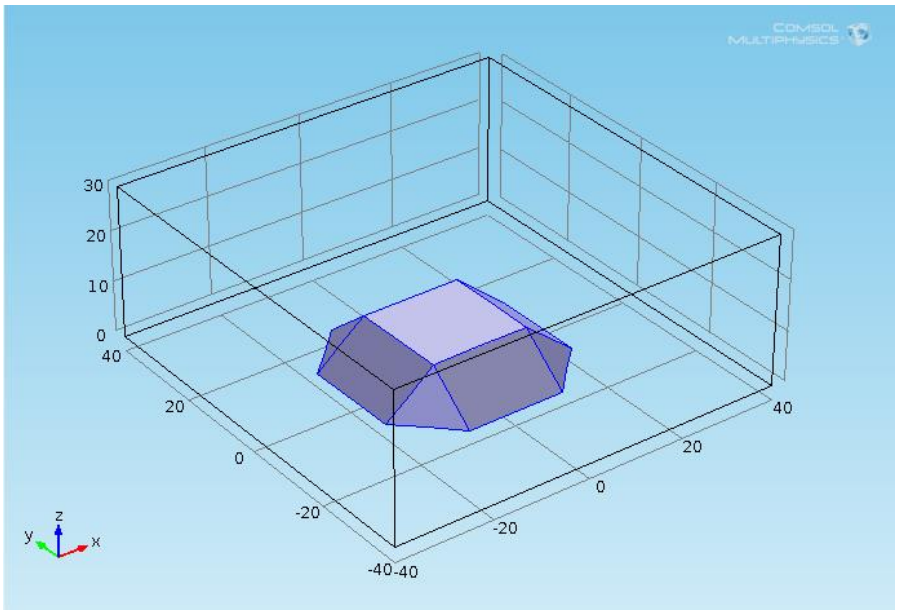

(a)

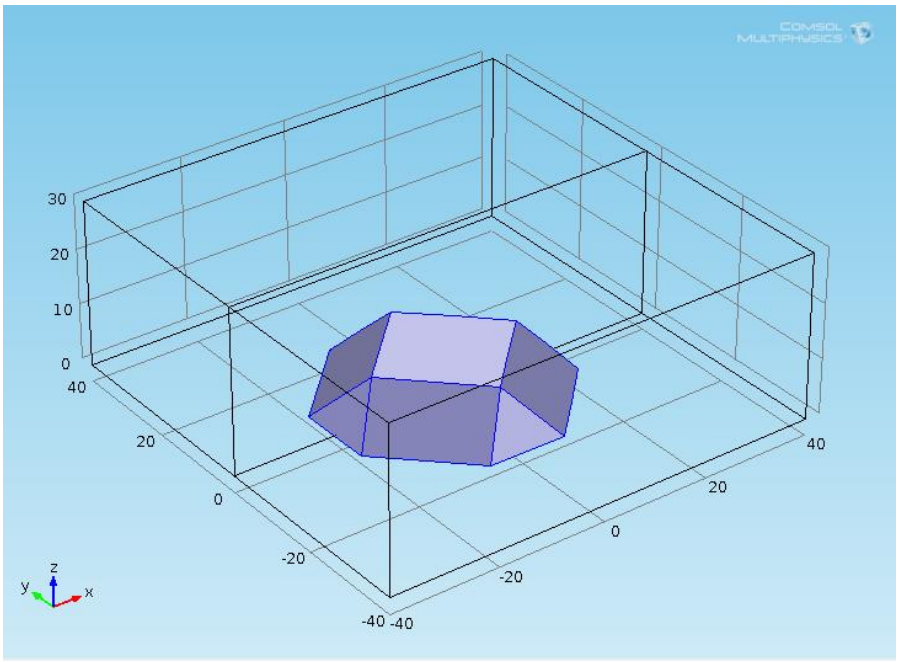

(b)

Figure 5.2 Geometry of an air storage container (unit: meter) with (a) parallel current and (b) diagonal current setups

The structure geometry and material properties is described in Table 5.1 and Table 5.2.

Table 5.1: Dimension parameters of the concrete structure

Concrete volume [m^3]	6030.1
Interior volume [m^3]	903.3
Bottom surface area [m^2]	1400

Table 5.2: Densities of TES materials

Materials	Density [kg/m^3]
Air (15˚C, 3MPa)	36.28
Concrete	2300
Sea Water	1025

The body force exerted on the air storage container due to the gravitational and buoyant force is described in two modes, water-filled mode and air-filled mode. The body force is also called as submerged weight. The body force in both modes can be estimated as follows:

$$\begin{aligned} F_{body} &= F_{buoyancy} + F_{gravity} \\ &= (-\rho_{water} g V_{air} - \rho_{water} g V_{concrete}) + (\rho_{air} g V_{air} + \rho_{concrete} g V_{concrete}) \\ &= (\rho_{air} - \rho_{water}) g V_{air} + (\rho_{concrete} - \rho_{water}) g V_{concrete} \end{aligned}$$

where ρ_x is density of material 'x', g is the gravitational constant, V_x is volume of material 'x'.

Table 5.3 shows the body force exerted on the concrete structure in each mode. (A positive sign represents the force acting upward)

Table 5.3: Body force exerted on the concrete structure on water-filled mode and air-filled mode

	Water-filled mode	Air-filled mode
Buoyant force [MN]	60.63	69.71
Gravitational force [MN]	-136.06	-136.38
Total Body force [MN]	-75.43	-66.67

The procedure of the simulation analysis is started from turbulent flow module with stationary mode. Having the data of pressure distribution on the surface of air storage container, the analysis using the structural mechanic module is performed consequently.

5.4. Results

Figure 5.3, 5.4, and 5.5 show the simulation results of the 3D velocity profiles and pressure distributions on the air storage container for parallel and diagonal currents at 0.1m/s, 1m/s, and 10 m/s, respectively.

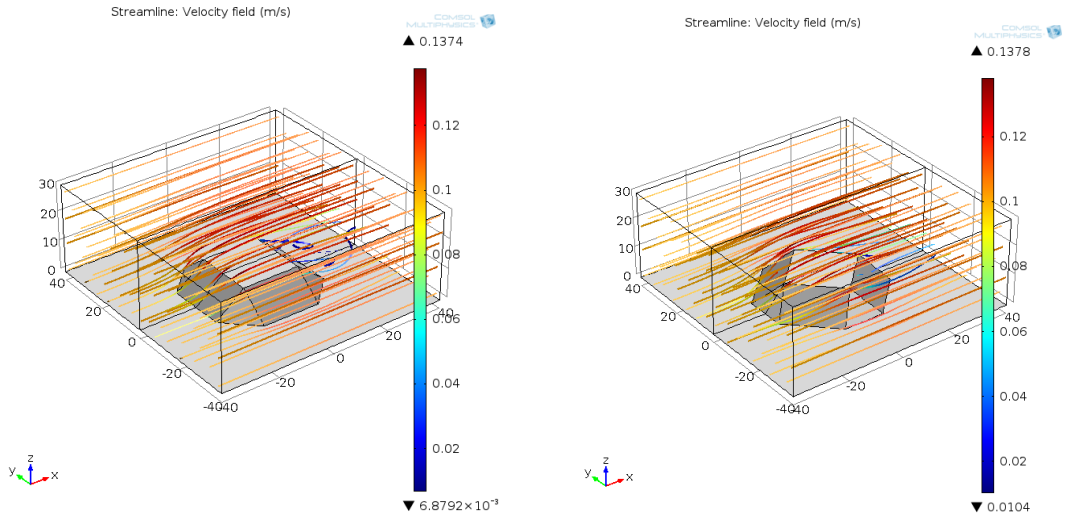

(a)

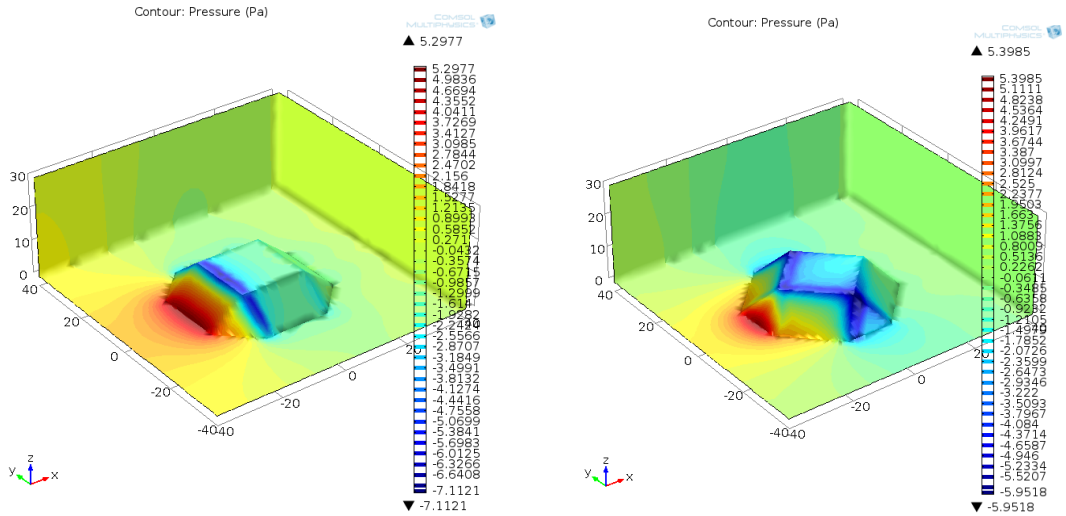

(b)

Figure 5.3 Results of (a) velocity profile and (b) pressure distribution at current speed of 0.1 m/s in parallel (left) and diagonal (right) direction

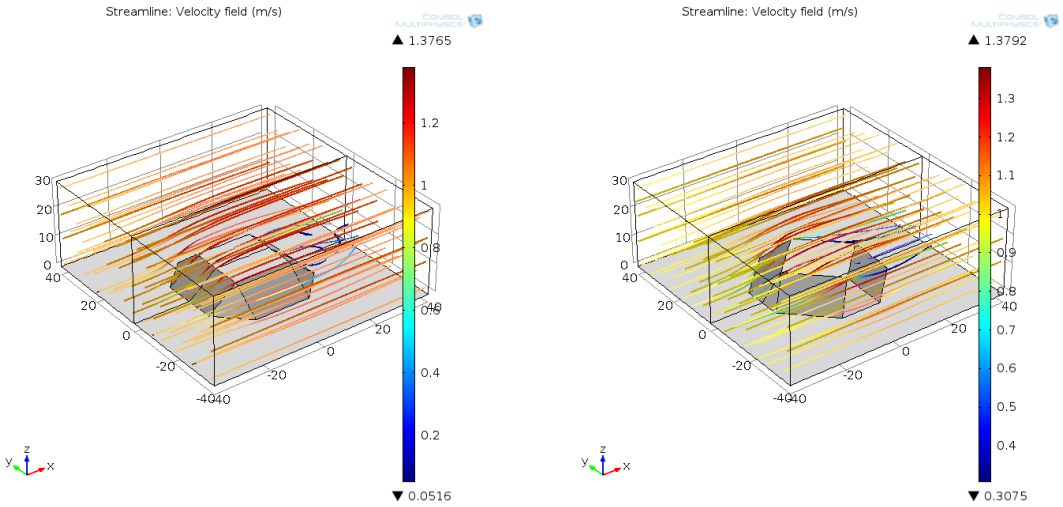

(a)

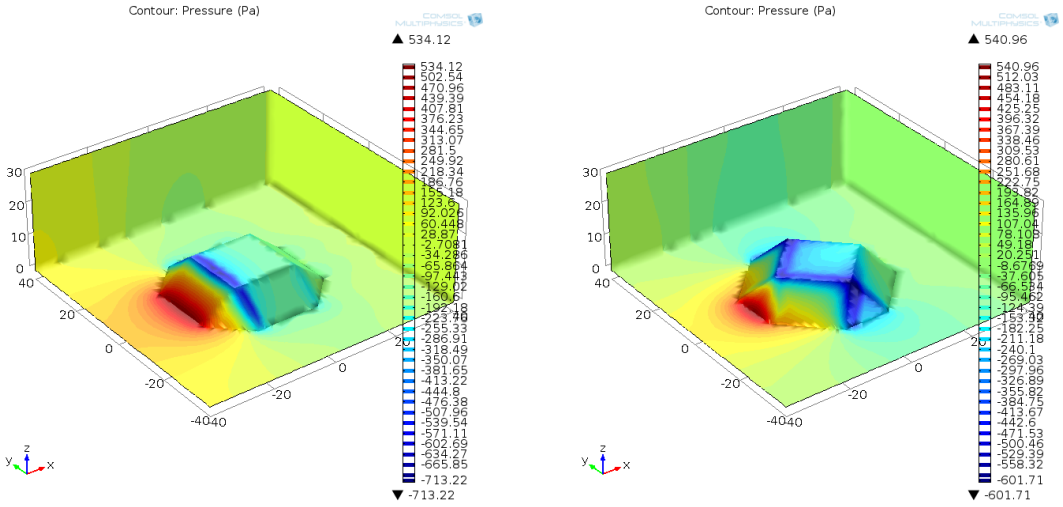

(b)

Figure 5.4 Results of (a) velocity profile and (b) pressure distribution at current speed of 1 m/s in parallel (left) and diagonal (right) direction

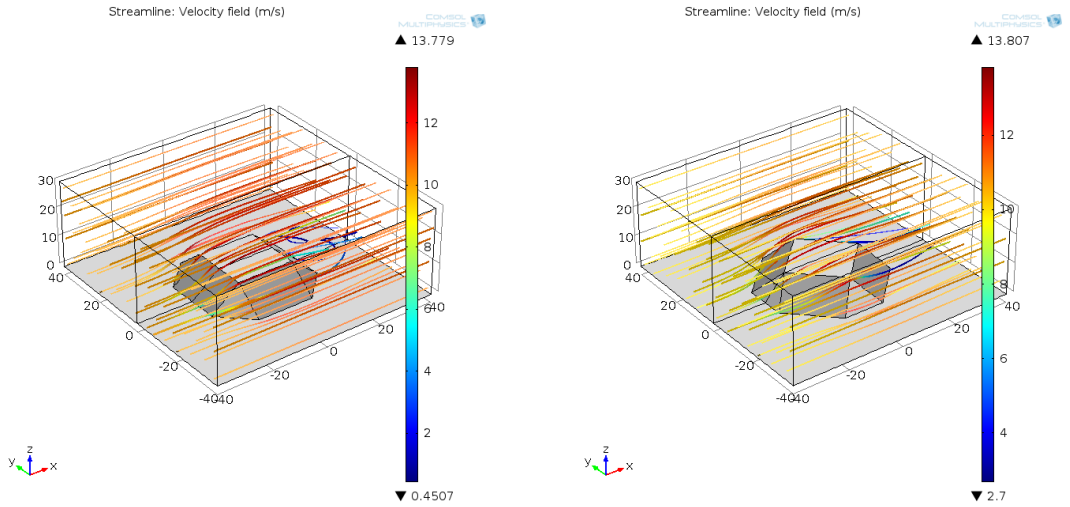

(a)

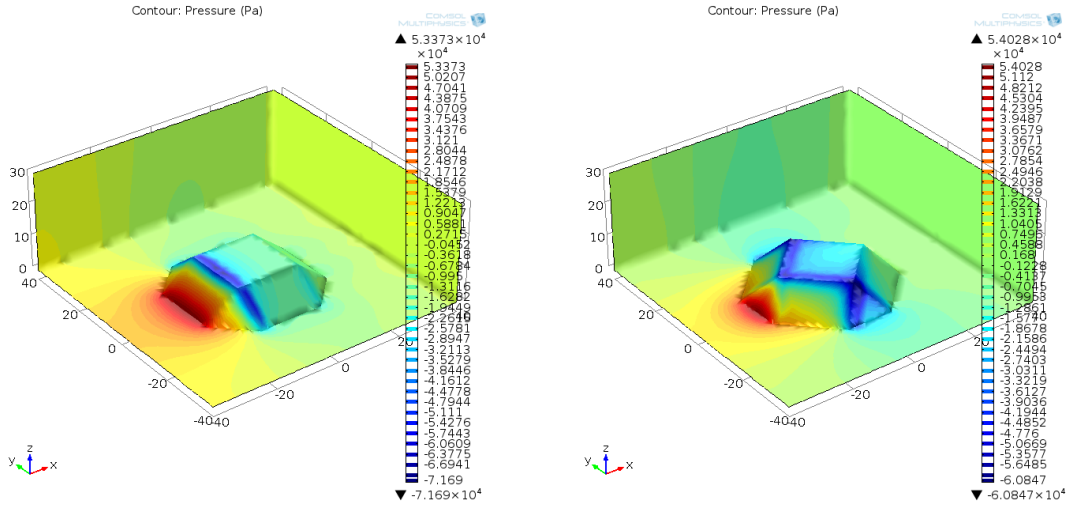

(b)

Figure 5.5 Results of (a) velocity profile and (b) pressure distribution at current speed of 10 m/s in parallel (left) and diagonal (right) direction

The flow velocity magnitudes increase by a factor of 10 from 0.1 m/s. And the velocity field and pressure distribution at three different velocities have a similar profiles for both parallel and diagonal directions.

Table 5.4 summarizes the numerical results from the simulations. In the table, the reaction force represents the force exerted to the air storage container by body force and flow-induced force. The lift force is the sum of z-directional reaction force and body force, which represents the upward force caused by flowing water.

Table 5.4: Numerical results of current flow simulations

	Setup		Body force	Reaction force		Lift force
			z - dir [kN]	x - dir [kN]	z - dir [kN]	z - dir [kN]
Parallel flow	0.1 [m/s]	Water-filled	-75422.98	-0.49	76870.00	1447.02
		Air-filled	-66661.567	-0.49	68300.00	1638.43
	1 [m/s]	Water-filled	-75422.98	-48.91	76720.00	1297.02
		Air-filled	-66661.567	-48.91	68180.00	1518.43
	10 [m/s]	Water-filled	-75422.98	-4861.00	61244.60	14178.38
		Air-filled	-66661.567	-4861.00	52710.00	13951.57
Diagonal flow	0.1 [m/s]	Water-filled	-75422.98	-0.44	76870.00	1447.02
		Air-filled	-66661.567	-0.44	68330.00	1668.43
	1 [m/s]	Water-filled	-75422.98	-44.73	76699.00	1276.02
		Air-filled	-66661.567	-44.73	68159.30	1497.73
	10 [m/s]	Water-filled	-75422.98	-4420.00	59030.00	16392.98
		Air-filled	-66661.567	-4420.00	50490.00	16171.57

In addition, the shear stress and normal stress on the seabed due to the gravitational, buoyant, and flow-induced forces are estimated in Table 5.5.

Table 5.5: Shear and normal stress induced on the seafloor under the concrete structure

	Setup		Shear stress	Normal Stress
			x - dir [kPa]	z - dir [kPa]
Parallel flow	0.1 [m/s]	Water-filled	0.00	-54.91
		Air-filled	0.00	-48.79
	1 [m/s]	Water-filled	0.03	-54.80
		Air-filled	0.03	-48.70
	10 [m/s]	Water-filled	3.47	-43.75
		Air-filled	3.47	-37.65
Diagonal flow	0.1 [m/s]	Water-filled	0.00	-54.91
		Air-filled	0.00	-48.81
	1 [m/s]	Water-filled	0.03	-54.76
		Air-filled	0.03	-48.69
	10 [m/s]	Water-filled	3.16	-42.16
		Air-filled	3.16	-36.06

In this data, the difference of the body forces between the air-filled and water-filled cases shows the buoyant force due to the compressed air. The maximum buoyant force of the compressed air is 11.6% of the body force based on the weight of the water-filled storage structure. It is shown that the change in the z-directional reaction force due to the current, which is named as the lift force, becomes significant as the current speed increases.

The worst-case scenario, as seen in Table 5.4, shows that the lift force due to a current velocity of 10m/s is 22.9% of the body force when the container is completely filled with air. Despite the fact that the x-direction reaction force over the container rises with the square of the flow velocity, the x-direction reaction force induced by a current velocity of 10m/s is still less than one-tenth of the z-direction reaction force. The friction force exerted between the container and the seabed can be obtained by the equation

$$F_f = \mu_s \cdot F_n$$

where F_f is the friction force, μ_s is the friction coefficient, and F_n is the normal force exerted on the air container. The friction coefficient between smooth concrete and seabed sand ranges between 0.60 to 0.67 (Bartholomew, 1992). Therefore, the static friction force with the lowest friction coefficient, 0.6, and the z-direction reaction force at the flow velocity of 10m/s, 50,490 kN, is calculated to be 30,294 kN. This shows that the storage structure would have a safety factor of 6.85 with respect to the magnitude of the x-direction reaction force at 10m/s, 4,420 kN, which is regarded as the largest drag force on the storage structure due to the flow. Therefore, the results imply the concrete storage model as currently designed will remain securely in place on the bottom of the ocean without any supplemental anchoring system.

5.5. Conclusion

Ocean flow simulations for underwater air storage system on the sea floor are conducted with various ocean current speeds. The ocean surface current velocity has reported to be up to 2.5 m/s (Adams, 1999). And during hurricane Sandy, which swept the United States eastern coast area in 2012, the maximum current speed at a depth of 3.8m was recorded to be 1.13m/s at the National Data Buoy Center station 44014, about 100 kilometers off the Virginia coast, on October 29th, 2012. To our knowledge, no data is available regarding flow velocity on the ocean floor (off the North Carolina coast) during a hurricane, so to be conservative our simulations use a flow velocity of 10 m/s.

As the result of the simulations, the concrete model under investigation in this study is found to be stable at current speeds up to 10 m/s. However, our simulations are based on the assumption that the seabed is flat and solid and does not take precise geotechnical details into consideration. It is also shown in the results section that there is the continuation of cyclic loading which can be up to 22.9% in change. Therefore, further research related to seabed deformation, stability, and disturbance of the container due to cyclic loading is ongoing in the department of Civil and Environmental Engineering at NCSU.

CHAPTER 6

CONCLUSIONS AND FUTURE RESEARCH

This research demonstrated a conceptual design of ocean compressed air energy storage (OCAES) system together with a thermodynamic model and current flow simulations for an air storage structure. The interest in offshore renewable energy is a trigger to recall the over-20-year technology, the CAES system. The overviews of existing CAES systems and its limitation have been presented and the thermodynamic analysis of the McIntosh plant has performed to collect more details of the operation conditions. The schematic of OCAES system has proposed after the consideration of available offshore renewable energy sources and geographical characteristics off the North Carolina coast. Based on the specifications of the McIntosh CAES plant, the thermodynamic OCAES model has been analyzed and its feasible configuration is presented with the required specifications of thermal energy storage and air storage container. The overall efficiency is estimated to be 58.7% and it is expected to be improved in conjunction with state-of-the-art turbomachinery, especially with high temperature compressors. In addition, the finite element analysis on the underwater air storage container designed by CCEE at NCSU has been carried out with current speeds of 0.1, 1, and 10 m/s. The simulation results under some restrictions show that the air storage structure would remain stable under such conditions.

Although the current studies on the overall OCAES system are as broad as possible, future work would require focusing on each subcomponent of the OCAES system. There would be

two major potential approaches which increase the efficiency of OCAES system. The first one is that, for an adiabatic OCAES system, a high temperature compressor train and an efficient heat exchanger would introduce the higher temperature to compressed air so that the overall energy recovery from compression to expansion would be improved. The second is to use an isothermal device for compression and expansion cycles. Unlike the massive TES in the adiabatic OCAES system, the isothermal device would significantly decrease the size of OCAES system. No isothermal compressor or expander unit is commercially developed so far. However, according to the results from the table-top model of isothermal compressor which is being developed by our project team, near-isothermal compression is positively anticipated for small-scale and low frequency cycles.

It is also noted that, since all components in the OCAES system is well developed so far, a comprehensive research on cost estimation models for the configuration and installation of the OCAES system would highly support to the feasibility of commercial application.

REFERENCES

Abele, A., Elkind, E., Intrator, J., & Washom, B. (2011). 2020 Strategic Analysis of Energy Storage in California: University of California, Berkeley School of Law; University of California, Los Angeles; and University of California, San Diego.

Adams, J. (1999). Ocean Currents *Microsoft Encarta Encyclopedia [CD-ROM]* (Vol. 2, pp. 191).

Arsie, I., Marano, V., Rizzo, G., & Moran, M. (2009). *Integration of wind turbines with compressed air energy storage.* Paper presented at the In AIP Conference Proceedings.

Bartholomew, C., Marsh, B., Hooper, R. (1992). *US Navy Salvage Engineer's Handbook* (Vol. 1): Washington D.C. Naval Sea Systems Command.

Basler, B., & Zaugg, Z. (1985). *Fuel flexibility in compressed air energy storage plants.* Paper presented at the 30th International Gas Turbine Conference and Exhibit., Houston, TX, USA.

Bejan, A. (2006). *Advanced engineering thermodynamics* (3rd ed.): Wiley New York.

Boehme, T., Cammaert, G., McCurry, J., Judt, M., & Deckers, M. (2007). *Windstore-large-scale energy storage offshore.* Paper presented at the Offshore Europe Conference, Aberdeen, UK.

Cheung, B., Cao, N., Carriveau, R., Ting, D. S. K. (2012). Distensible air accumulators as a means of adiabatic underwater compressed air energy storage. *International Journal of Environmental Studies, 69*(4), 566-577.

Coney, M. W., Stephenson, P., Malmgren, A., Linnemann, C., Morgan, R. E., Richards, R. A., ... & Abdallah, H. (2002). *Development of a reciprocating compressor using water injection to achieve quasi-isothermal compression*. Paper presented at the the 16th International Compressor Engineering Conference, West Lafayette, IN.

Crotogino, F., Mohmeyer, K. U., & Scharf, R. (2001). *Huntorf CAES: More than 20 years of successful operation.* Paper presented at the Proceedings of SMRI Spring Meeting.

Denholm, P. (2006). Improving the technical, environmental and social performance of wind energy systems using biomass-based energy storage. *Renewable Energy, 31*(9), 1355-1370.

Desai, N., Gonzalez, S., Pemberton, D., & Rathjen, T. (2005). The economic impact of CAES on wind in TX, OK, and NM. Texas State Energy Conservation Office Ridge Energy Storage & Grid Services L.P.

Dresser-Rand. (2010). Compressed Air Energy Storage (CAES). Retrieved from www.dresser-rand.com

E.ON. (2013). Fact & Figures. Huntorf Power Plant Retrieved Feb 18, 2013, from http://www.kraftwerk-wilhelmshaven.com/

EIA. (2011). Annual energy review. Washington, DC: Energy Information Administration, US Department of Energy.

Eilperin, J. (2010). Offshore wind farm near Cape Cod, first in US, gets federal approval, *The Washington Post*.

Favret, F. (2004). Up-to-Date Researches and Future Trends in Underground Gas Storage Facillties: A State of the Art Review. *Security of natural gas supply through transit countries*, 159-193.

Garrison, J. B., Kapner, M., & Webber, M. E. (2009). *A First order thermodynamic and economic analysis for integrating thermal and compressed air energy storage for a dispatchable wind and solar powered system.* Paper presented at the ASME 3rd International Conference on Energy Sustainability, ES2009, San Francisco, CA, USA.

Garrison, J. B., & Webber, M. E. (2011). An integrated energy storage scheme for a dispatchable solar and wind powered energy system. *Journal of Renewable and Sustainable Energy, 3*(4), 043101.

Gil, A., Medrano, M., Martorell, I., Lázaro, A., Dolado, P., Zalba, B., & Cabeza, L. F. (2010). State of the art on high temperature thermal energy storage for power generation. Part 1—Concepts, materials and modellization. *Renewable and Sustainable Energy Reviews, 14*(1), 31-55.

Grazzini, G., & Milazzo, A. (2008). Thermodynamic analysis of CAES/TES systems for renewable energy plants. *Renewable Energy, 33*(9), 1998-2006.

Hartmann, N., Vöhringer, O., Kruck, C., & Eltrop, L. (2012). Simulation and analysis of different adiabatic Compressed Air Energy Storage plant configurations. *Applied Energy, 93*, 541-548.

Hugenroth, J., Braun, J., Groll, E., & King, G. (2007). Thermodynamic analysis of a liquid-flooded Ericsson cycle cooler. *International Journal of Refrigeration, 30*(7), 1176-1186.

Ibrahim, H., Basbous, T., Ilinca, A., & Dimitrova, M. (2011). Optimization of diesel engine performances for a hybrid wind-diesel system with compressed air energy storage. *Energy, 36*(5), 3079-3091.

Jakiel, C., Zunft, S., & Nowi, A. (2007). Adiabatic compressed air energy storage plants for efficient peak load power supply from wind energy: the European project AA-CAES. *International Journal of Energy Technology and Policy, 5*(3), 296-306.

Kearney, D., Herrmann, U., Nava, P., Kelly, B., Mahoney, R., Pacheco, J., ... & Price, H. (2003). Assessment of a molten salt heat transfer fluid in a parabolic trough solar field. *TRANSACTIONS-AMERICAN SOCIETY OF MECHANICAL ENGINEERS JOURNAL OF SOLAR ENERGY ENGINEERING, 125*(2), 170-176.

Keim, B. D., Muller, R. A., & Stone, G. W. (2007). Spatiotemporal patterns and return periods of tropical storm and hurricane strikes from Texas to Maine. *Journal of Climate, 20*(14), 3498-3509.

Laing, D., Lehmann, D., Fiss, M., & Bahl, C. (2009). Test results of concrete thermal energy storage for parabolic trough power plants. *Journal of Solar Energy Engineering(Transactions of the ASME), 131*(4).

Laing, D., Steinmann, W. D., Tamme, R., & Richter, C. (2006). Solid media thermal storage for parabolic trough power plants. *Solar energy, 80*(10), 1283-1289.

McAllister, E. W. (2009). *Pipeline rules of thumb handbook: a manual of quick, accurate solutions to everyday pipeline engineering problems*: Gulf Professional Publishing.

Medrano, M., Gil, A., Martorell, I., Potau, X., & Cabeza, L. F. (2010). State of the art on high-temperature thermal energy storage for power generation. Part 2—Case studies. *Renewable and Sustainable Energy Reviews, 14*(1), 56-72.

Milborrow, D. (2003). Offshore wind rises to the challenge, *Windpower Monthly Magazine*.

Musial, W., & Butterfield, S. (2004). *Future for offshore wind energy in the United States.* Paper presented at the EnergyOcean 2004 Conference, Palm Beach, Florida.

Musial, W., & Ram, B. (2010). Large-scale offshore windpower in the United States: Assessment of oppportunities and barriers: NREL.

Nikolaos, N. (2004). *Deep water offshore wind technologies.* Master thesis, University of Strathclyde.

NOAA. (2011). Chart 1220: National Oceanic and Atmospheric Administration.

Pimm, A., & Garvey, S. (2009). *Analysis of flexible fabric structures for large-scale subsea compressed air energy storage.* Paper presented at the 7th International Conference on Modern Practice in Stress and Vibration Cambridge, UK.

Pimm, A. J. (2011). *Analysis of flexible fabric structures.* Doctoral dissertation, University of Nottingham.

Pollak, R. (1994a). History of first US compressed-air energy storage (CAES) plant (110 MW 26h) volume 1: Early CAES development: Electric Power Research Institute (EPRI).

Pollak, R. (1994b). History of first US compressed-air energy storage (CAES) Plant (110 MW 26h) volume 2: Construction: Electric Power Research Institute (EPRI).

Rastler, D. M. (2010). Electricity Energy Storage Technology Options: A White Paper Primer on Applications, Costs and Benefits: Electric Power Research Institute.

Rebours, Y., & Kirschen, D. (2005). What is spinning reserve: The University of Manchester.

Rice, A. T. (2011). *Heat transfer enhancement in a cylindrical compression chamber by way of porous inserts and the optimization of compression and expansion trajectories for varying heat transfer capabilities.* Master Thesis, University of Minnesota.

Schainker, R., Pollak, R., & Mehta, B. (1993). *Overview of CAES technology.* Paper presented at the Proceedings of the American Power Conference, Chicago, IL, USA.

Self, C. (2011). Dishonorable Disposal - The Case Against Dumping U.S. Naval Vessels at Sea: Basel Action Network.

Seymour, R. J. (1997). *Undersea pumped storage for load leveling.* Paper presented at the Proceedings of the 1997 Conference on California and the World Ocean. Part 1 (of 2), San Diego, CA, USA.

Seymour, R. J. (2007). *Ocean energy on-demand using underocean compressed air storage.* Paper presented at the 26th International Conference on Offshore Mechanics and Arctic Engineering 2007, OMAE2007, San Diego, CA, USA.

Seymour, R. J. (2012). [Personal Communication].

Singal, R. K. (1984). Theory and design of compressed air storage plants. *Electrical India, 24*(19), 5-8.

Steta, F. D. S. (2010). *Modeling of an advanced adiabatic compressed air energy storage (AA-CAES) unit and an optimal model-based operation strategy for its integration into power markets.* Masters Thesis, Swiss Federal Institute of Technology (ETH) Zurich.

Succar, S., Williams, R. H. (2008). Compressed air energy storage: Theory, resources, and applications for wind power *Princeton Environmental Institute Report* (Vol. 8).

TheEconomist. (2012). Packing some power *Technology Quarterly* (Vol. Q1): The Economist.

Tuschy, I. A., R.; Gerdes, R.; Keller-Sornig, P. . (2002). Compressed air energy storage with high efficiency and power output. *VDI Berichte*(1734), 57-66.

Uken, M. (Producer). (2012, Feb 18, 2013). Effizienter Druckluftspeicher l ässt auf sich warten. *Zeit Online*.

Van de Ven, J. D., & Li, P. Y. (2009). Liquid piston gas compression. *Applied Energy, 86*(10), 2183-2191.

Zunft, S., Jakiel, C., Koller, M., & Bullough, C. (2006). *Adiabatic compressed air energy storage for the grid integration of wind power.* Paper presented at the Sixth International Workshop on Large-Scale Integration of Wind Power and Transmission Networks for Offshore Windfarms, Delft, the Netherlands.

APPENDICES

Appendix A

COMSOL 4.3a settings and modes: Current flowing simulation

A.1 Setting

A.1.1 Parameters

Name	Expression	Description
u_mean	10[m/s]	
v_a	903.264	interior volume
load1	-(2300-1025)*(6933-903.3)[kg]*g_const	body load when water filled
load2	-(2300-1025)* (6933-903.3)[kg]*g_const + (1025 - 36)*903.3[kg]*g_const	body load when air filled
theta	0	facing angle of the structure (0, 45)

A.1.2 Geometry

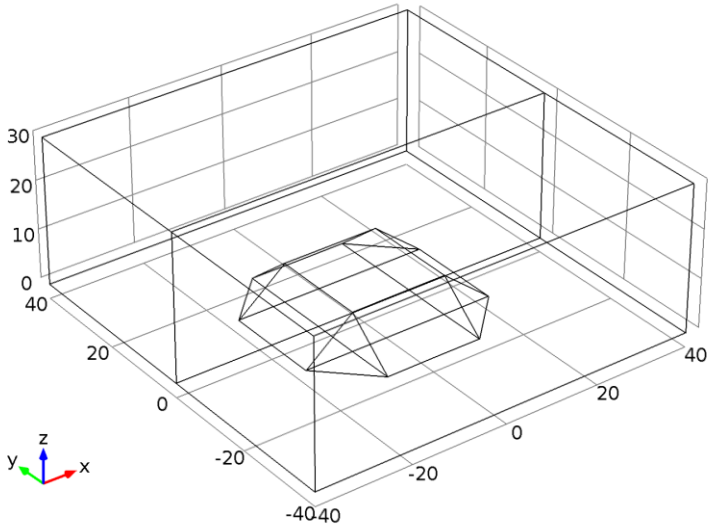

A.1.3 Materials

A.1.3.1 Concrete

Material parameters

Name	Value	Unit
Density	2300[kg/m^3]	kg/m^3
Young's modulus	25e9[Pa]	Pa
Poisson's ratio	0.33	1

Basic Settings

Description	Value
Coefficient of thermal expansion	{{10e-6[1/K], 0, 0}, {0, 10e-6[1/K], 0}, {0, 0, 10e-6[1/K]}}
Density	2300[kg/m^3]
Thermal conductivity	{{1.8[W/(m*K)], 0, 0}, {0, 1.8[W/(m*K)], 0}, {0, 0, 1.8[W/(m*K)]}}

Young's modulus and Poisson's ratio Settings

Description	Value
Young's modulus	25e9[Pa]
Poisson's ratio	0.33

A.1.3.2 Air

Basic Settings

Description	Value
Dynamic viscosity	eta(T[1/K])[Pa*s]
Ratio of specific heats	1.4
Electrical conductivity	{{0[S/m], 0, 0}, {0, 0[S/m], 0}, {0, 0, 0[S/m]}}
Heat capacity at constant pressure	Cp(T[1/K])[J/(kg*K)]
Density	rho(pA[1/Pa], T[1/K])[kg/m^3]
Thermal conductivity	{{k(T[1/K])[W/(m*K)], 0, 0}, {0, k(T[1/K])[W/(m*K)], 0}, {0, 0, k(T[1/K])[W/(m*K)]}}
Speed of sound	cs(T[1/K])[m/s]

A.1.3.3 Water

Material parameters

Name	Value	Unit
Dynamic viscosity	eta(T[1/K])[Pa*s]	Pa*s
Density	rho(T[1/K])[kg/m^3]	kg/m^3

Basic Settings

Description	Value
Dynamic viscosity	eta(T[1/K])[Pa*s]
Ratio of specific heats	1.0
Electrical conductivity	{{5.5e-6[S/m], 0, 0}, {0, 5.5e-6[S/m], 0}, {0, 0, 5.5e-6[S/m]}}
Heat capacity at constant pressure	Cp(T[1/K])[J/(kg*K)]
Density	rho(T[1/K])[kg/m^3]
Thermal conductivity	{{k(T[1/K])[W/(m*K)], 0, 0}, {0, k(T[1/K])[W/(m*K)], 0}, {0, 0, k(T[1/K])[W/(m*K)]}}
Speed of sound	cs(T[1/K])[m/s]

A.1.4 Turbulent Flow, k-ε (spf)

Selection

Geometric entity level	Domain
Selection	Domains 1–2

Equations

$$\rho(\mathbf{u}\cdot\nabla)\mathbf{u} = \nabla\cdot\left[-p\mathbf{I}+(\mu+\mu_T)\left(\nabla\mathbf{u}+(\nabla\mathbf{u})^T\right)-\frac{2}{3}\rho k\mathbf{I}\right]+\mathbf{F}$$

$$\rho\nabla\cdot\mathbf{u}=0$$

$$\rho(\mathbf{u}\cdot\nabla)k=\nabla\cdot\left[\left(\mu+\frac{\mu_T}{\sigma_k}\right)\nabla k\right]+P_k-\rho\varepsilon$$

$$\rho(\mathbf{u}\cdot\nabla)\varepsilon=\nabla\cdot\left[\left(\mu+\frac{\mu_T}{\sigma_\varepsilon}\right)\nabla\varepsilon\right]+C_{\varepsilon 1}\frac{\varepsilon}{k}P_k-C_{\varepsilon 2}\rho\frac{\varepsilon^2}{k},\quad \varepsilon=\mathrm{ep}$$

$$\mu_T=\rho C_\mu\frac{k^2}{\varepsilon}$$

$$P_k = \mu_T\left[\nabla\mathbf{u} : \left(\nabla\mathbf{u} + (\nabla\mathbf{u})^T\right)\right]$$

Settings

Description	Value
Compressibility	Incompressible flow
Use pseudo time stepping for stationary equation form	1
CFL number expression	Manual
Local CFL number	3 + if(niterCMP>=15, 1.3^min(niterCMP - 15, 7), 0) + if(niterCMP>=40, 9*1.3^min(niterCMP - 40, 9), 0) + if(niterCMP>=70, 90*1.3^min(niterCMP - 70, 9), 0)
Turbulence model type	RANS
Show equation assuming	std1/stat
Allow out of plane properties	0
Allow stokes properties	0

Used products

COMSOL Multiphysics
CFD Module

A.1.4.1 Fluid Properties 1

Selection

Geometric entity level	Domain
Selection	Domains 1–2

Equations

$$\rho(\mathbf{u}\cdot\nabla)\mathbf{u} =$$

$$\nabla\cdot\left[-p\mathbf{I} + (\mu+\mu_T)\left(\nabla\mathbf{u} + (\nabla\mathbf{u})^T\right) - \frac{2}{3}\rho k\mathbf{I}\right] + \mathbf{F}$$

$$\rho\nabla\cdot\mathbf{u} = 0$$

$$\rho(\mathbf{u}\cdot\nabla)k = \nabla\cdot\left[\left(\mu + \frac{\mu_T}{\sigma_k}\right)\nabla k\right] + P_k - \rho\varepsilon$$

$$\rho(\mathbf{u}\cdot\nabla)\varepsilon = \nabla\cdot\left[\left(\mu + \frac{\mu_T}{\sigma_\varepsilon}\right)\nabla\varepsilon\right] + C_{\varepsilon 1}\frac{\varepsilon}{k}P_k - C_{\varepsilon 2}\rho\frac{\varepsilon^2}{k}, \quad \varepsilon = \mathrm{ep}$$

Properties from material

Property	Material	Property group
Density	Water	Basic
Dynamic viscosity	Water	Basic

A.1.4.2 Wall 1

Selection

Geometric entity level	Boundary
Selection	Boundaries 3, 7, 11–13, 16–24

Equations

$$\mathbf{u}\cdot\mathbf{n} = 0$$

$$\left[(\mu+\mu_T)\left(\nabla\mathbf{u} + (\nabla\mathbf{u})^T\right) - \frac{2}{3}\rho k\mathbf{I}\right]\mathbf{n} = -\rho\frac{u_\tau}{\delta_w^+}\mathbf{u}_{tang}$$

$$\mathbf{u}_{tang} = \mathbf{u} - (\mathbf{u}\cdot\mathbf{n})\mathbf{n}$$

$$\nabla k\cdot\mathbf{n} = 0, \quad \varepsilon = \rho\frac{C_\mu k^2}{\kappa_v\delta_w^+\mu}$$

A.1.4.3 Inlet 1

Selection

Geometric entity level	Boundary
Selection	Boundaries 1, 5

Equations

$$\mathbf{u} = -U_0\mathbf{n}$$

$$k = \frac{3}{2}(U_0 I_T)^2, \quad \epsilon = C_\mu^{3/4}\frac{k^{3/2}}{L_T}$$

Settings

Settings

Description	Value
Normal inflow velocity	u_mean
Turbulence length scale	10[m]

A.1.4.4 Outlet 1

Selection

Geometric entity level	Boundary
Selection	Boundaries 25–26

Equations

$$p = p_0, \quad \left[(\mu + \mu_T)\left(\nabla\mathbf{u} + (\nabla\mathbf{u})^T\right) - \frac{2}{3}\rho k\mathbf{I}\right]\cdot\mathbf{n} = \mathbf{0}$$

$$\nabla k\cdot\mathbf{n} = 0, \quad \nabla\epsilon\cdot\mathbf{n} = 0$$

A.1.4.5 Wall 2

Selection

Geometric entity level	Boundary
Selection	Boundaries 2, 4, 8–9

Equations

$$\mathbf{u}\cdot\mathbf{n} = 0, \quad \mathbf{K} - (\mathbf{K}\cdot\mathbf{n})\mathbf{n} = \mathbf{0}$$

$$\mathbf{K} = \left[(\mu + \mu_T)\left(\nabla\mathbf{u} + (\nabla\mathbf{u})^T\right) - \frac{2}{3}\rho k\mathbf{I}\right]\mathbf{n}$$

$$\nabla k\cdot\mathbf{n} = 0, \quad \nabla\epsilon\cdot\mathbf{n} = 0$$

Settings

Settings

Description	Value
Boundary condition	Slip

A.1.5 Solid Mechanics (solid)

Selection

Geometric entity level	Domain
Selection	Domains 3–4

Equations

$$-\nabla\cdot\sigma = \mathbf{F}_V$$

Settings

Description	Value
Structural transient behavior	Quasi - static
Show equation assuming	std1/stat

A.1.5.1 Linear Elastic Material Model 1

Selection

Geometric entity level	Domain

Selection	Domains 3–4

Equations

$$-\underline{\underline{\nabla \cdot \sigma}} = \mathbf{F_V}, \quad \sigma = J^{-1}\mathbf{F}\underline{\underline{S}}\mathbf{F}^T, \quad \mathbf{F} = \left(\mathbf{I} + \nabla \mathbf{u2}\right), \quad J = \det(\mathbf{F})$$

$$\underline{\underline{S}} - \underline{\underline{S_0}} = \underline{\underline{\underline{\underline{C}}}} : (\underline{\underline{\epsilon}} - \underline{\underline{\epsilon_0}} - \underline{\underline{\epsilon_{inel}}}) - (\mathrm{trace}(\underline{\underline{\underline{\underline{C}}}} : (\underline{\underline{\epsilon}} - \underline{\underline{\epsilon_0}} - \underline{\underline{\epsilon_{inel}}}))/3 + p_w)\mathbf{I}$$

$$\underline{\underline{\epsilon}} = \frac{1}{2}\left[(\nabla \mathbf{u2})^T + \nabla \mathbf{u2} + (\nabla \mathbf{u2})^T \nabla \mathbf{u2}\right]$$

Settings

Settings

Description	Value
Nearly incompressible material	On

Properties from material

Property	Material	Property group
Young's modulus	Concrete	Young's modulus and Poisson's ratio
Poisson's ratio	Concrete	Young's modulus and Poisson's ratio
Density	Concrete	Basic

A.1.5.2 Free 1

Selection

Geometric entity level	Boundary
Selection	No boundaries

A.1.5.3 Body Load 1

Selection

Geometric entity level	Domain
Selection	Domains 3–4

Equations

$$-\nabla \cdot \sigma = \underline{\underline{\mathbf{F_V}}}$$

$$\mathbf{F_V} = \frac{\mathbf{F_{tot}}}{V}$$

A.1.5.4 Boundary Load 1

Selection

Geometric entity level	Boundary
Selection	Boundaries 11–13, 16–24

Equations

$$\sigma \cdot \mathbf{n} = \underline{\underline{\mathbf{F_A}}}$$

A.1.5.5 Fixed Constraint 1

Selection

Geometric entity level	Boundary
Selection	Boundaries 10, 14

Equations

$$\underline{\underline{\mathbf{u2} = \mathbf{0}}}$$

A.1.6 Mesh 1

Mesh statistics

Property	Value
Minimum element quality	0.2398
Average element quality	0.77
Tetrahedral elements	145702
Triangular elements	8921

Property	Value
Edge elements	507
Vertex elements	28

A.1.6.1 Size (size)
Settings

Name	Value
Maximum element size	2.8
Minimum element size	0.12
Resolution of curvature	0.3
Resolution of narrow regions	0.85
Maximum element growth rate	1.35
Predefined size	Extra fine

A.2 Study 1

A.2.1 Parametric Sweep
Parameter name: u_mean
Parameters: 0.1, 1, 10

A.2.2 Stationary
Mesh selection

Geometry	Mesh
Geometry 1 (geom1)	mesh1

Physics selection

Physics	Discretization
Turbulent Flow, k-ε (spf)	physics

A.2.3 Solver Configurations
A.2.3.1 Solver 1
Compile Equations: Stationary (st1)
Study and step

Name	Value
Use study	Study 1
Use study step	Stationary

Dependent Variables 1 (v1)
General

Name	Value
Defined by study step	Stationary

Initial values of variables solved for

Name	Value
Solution	Zero

Values of variables not solved for

Name	Value
Solution	Zero

mod1.u (mod1_u)
General

Name	Value
Field components	{mod1.u, mod1.v, mod1.w}

mod1.p (mod1_p)
General

Name	Value
Field components	mod1.p

mod1.solid.pw (mod1_solid_pw)
General

Name	Value
Field components	mod1.solid.pw
Solve for this field	Off

mod1.u2 (mod1_u2)
General

Name	Value
Field components	{mod1.u2, mod1.v2, mod1.w2}
Solve for this field	Off

mod1.k (mod1_k)
General

Name	Value
Field components	mod1.k

mod1.ep (mod1_ep)
General

Name	Value
Field components	mod1.ep

Stationary Solver 1 (s1)
General

Name	Value
Defined by study step	User defined

Parametric 1 (p1)
General

Name	Value
Defined by study step	Parametric Sweep
Parameter value list	0.1, 1, 10

Segregated 1 (se1)
Segregated Step 1 (ss1)
General

Name	Value
Variables	{mod1.u, mod1.p}
Linear solver	Iterative 1

Segregated Step 2 (ss2)
General

Name	Value
Variables	{mod1.k, mod1.ep}
Linear solver	Iterative 2

Lower Limit 1 (ll1)
Lower limit

Name	Value
Lower limits (field variables)	mod1.k 0 mod1.ep 0

Iterative 1 (i1)

Error

Name	Value
Factor in error estimate	20
Maximum number of iterations	200
Nonlinear based error norm	On

Multigrid 1 (mg1)
Presmoother (pr)
SOR Line 1 (sl1)
Main

Name	Value
Relaxation factor	0.3
Line based on	Matrix
Multivariable method	Coupled
Line variable	mod1.u
Maximum line length	15

Secondary

Name	Value
Relaxation factor	0.3

Postsmoother (po)
SOR Line 1 (sl1)
Main

Name	Value
Relaxation factor	0.4
Line based on	Matrix
Multivariable method	Coupled
Line variable	mod1.u
Maximum line length	15

Secondary

Name	Value
Number of secondary iterations	2
Relaxation factor	0.5

Coarse Solver (cs)
Direct 1 (d1)
General

Name	Value
Solver	PARDISO

Iterative 2 (i2)
Error

Name	Value
Maximum number of iterations	200
Nonlinear based error norm	On

Multigrid 1 (mg1)
Presmoother (pr)
SOR Line 1 (sl1)
Main

Name	Value
Relaxation factor	0.3

Secondary

Name	Value

Name	Value
Relaxation factor	0.3

Postsmoother (po)
SOR Line 1 (sl1)
Main

Name	Value
Relaxation factor	0.4

Secondary

Name	Value
Number of secondary iterations	2
Relaxation factor	0.5

Coarse Solver (cs)
Direct 1 (d1)
General

Name	Value
Solver	PARDISO

A.3 Study 2

A.3.1 Stationary

Mesh selection

Geometry	Mesh
Geometry 1 (geom1)	mesh1

Physics selection

Physics	Discretization
Solid Mechanics (solid)	physics

A.3.2 Solver Configurations

A.3.2.1 Solver 2

Compile Equations: Stationary (st1)
Study and step

Name	Value
Use study	Study 2
Use study step	Stationary

Dependent Variables 1 (v1)
General

Name	Value
Defined by study step	Stationary

Initial values of variables solved for

Name	Value
Method	Solution
Solution	Solver 3

Values of variables not solved for

Name	Value
Method	Solution
Solution	Solver 3

mod1.u (mod1_u)
General

Name	Value
Field components	{mod1.u, mod1.v, mod1.w}

Name	Value
Solve for this field	Off

mod1.p (mod1_p)
General

Name	Value
Field components	mod1.p
Solve for this field	Off

mod1.solid.pw (mod1_solid_pw)
General

Name	Value
Field components	mod1.solid.pw

mod1.u2 (mod1_u2)
General

Name	Value
Field components	{mod1.u2, mod1.v2, mod1.w2}

mod1.k (mod1_k)
General

Name	Value
Field components	mod1.k
Solve for this field	Off

mod1.ep (mod1_ep)
General

Name	Value
Field components	mod1.ep
Solve for this field	Off

Stationary Solver 1 (s1)
General

Name	Value
Defined by study step	Stationary

Fully Coupled 1 (fc1)
General

Name	Value
Linear solver	Direct